pH-Controlled Photochromism of Hydroxyflavylium Ions

Fernando Pina,* Maria João Melo, A. Jorge Parola, Mauro Maestri,* and Vincenzo Balzani*

Abstract: The structural transformations and photochromic properties of the 7-hydroxyflavylium ion have been investigated by means of the pH jump technique and continuous and pulsed light excitation. The primary photoproduct of UV irradiation of the colorless *trans*-chalcone form, which is the predominant species at pH 4, is its colorless *cis* isomer, which rapidly disappears on a time scale of seconds through two competitive processes: i) back-reaction to yield the *trans*-chalcone form, and ii) formation of the colored flavylium ion and its conjugated quinoidal base. Over minutes or hours (depending on pH), the system reverts quantitatively to its original state. The rate constants and equilibrium constants of the various processes have been obtained and compared with those previously reported for the 4′-hydroxyflavylium and 4′,7-dihydroxyflavylium ions. This comparison demonstrates the substituent effect on the rate and equilibrium constants; the effect on the rate constant of the *cis* → *trans* thermal isomerization reaction is particularly strong. For the 7-hydroxyflavylium and 4′,7-dihydroxyflavylium ions the pH of the solution plays the role of a tap for the color intensity generated by light excitation. This also means that this system can be viewed as a light-switchable pH indicator.

Keywords: flash photolysis · flavylium salts · kinetics · photochromism · UV/Vis spectroscopy

Introduction

The synthetic flavylium salts have a basic chemical structure identical to the anthocyanins, one of the most important families of colorants of flowers and fruits.[1–6] Previous systematic investigations[5–6] have shown that in acidic and neutral aqueous solution flavylium ions undergo complex structural transformations that, in the case of the 7-hydroxyflavylium ion, the object of the present work, can be represented as in Scheme 1. Such transformations, which are accompanied by changes in the UV/Vis absorption and emission spectra of the solution, can be induced by pH changes and/or by light excitation and can be studied by using the pH jump and continuous and flash photolysis techniques.[7–11] Of particular interest is the reversible photoinduced isomerization of the thermally stable (within a certain pH range) *trans*-chalcone form, which in the case of the 4′-methoxyflavylium ion can initiate a *write-lock-read-unlock-erase* photochromic cycle for information processing.[10] More recently it has been shown that in the case of 4′-hydroxyflavylium ion the light- and/or pH-induced transformations

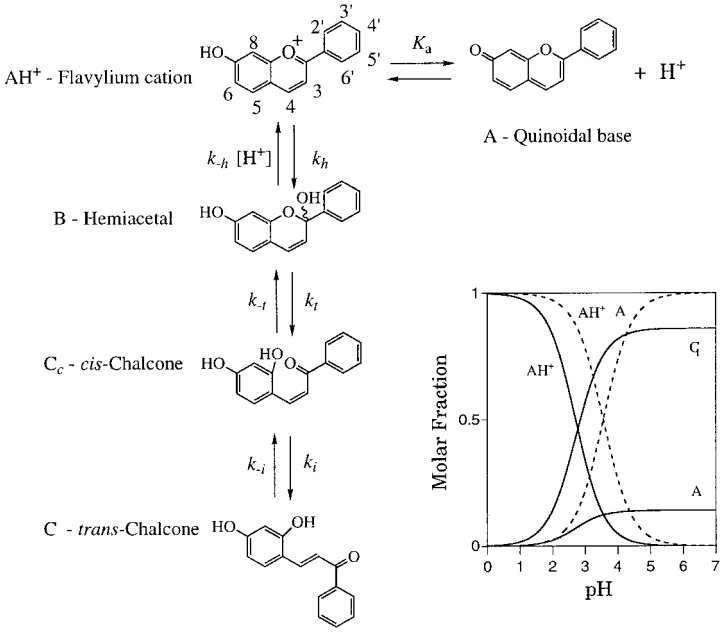

Scheme 1. Kinetic scheme describing the structural transformations taking place in the 7-hydroxyflavylium system. Inset: molar fraction distributions of the various species present at the thermodynamic equilibrium (solid lines) and immediately after pH jumps starting from pH 1.0 (dashed lines).

[*] Prof. F. Pina, Dr. M. J. Melo, A. J. Parola
Departamento de Química, Centro de Química Fina e Biotecnologia
Universidade Nova de Lisboa,
2825 Monte de Caparica (Portugal)
E-mail: fjp@dq.fct.unl.pt

Prof. M. Maestri, Prof. V. Balzani
Dipartimento di Chimica G. Ciamician, Università di Bologna
Via Selmi 2, 40126 Bologna (Italy)
Fax: (+39) 51-259456
E-mail: mmaestri@ciam.unibo.it
E-mail: vbalzani@ciam.unibo.it

  0947-6539/98/0410-2001 $ 17.50+.25/0

can also be taken as a basis for simple logic operations and form a remarkably intricate network of chemical processes.[11]

In this paper we report the results of an investigation carried out on the 7-hydroxyflavylium ion. The rate constants and equilibrium constants of the various processes have been obtained and compared with those previously reported for the 4′-hydroxyflavylium and 4′,7-dihydroxyflavylium ions. Some peculiar properties related to the interconnections between the pH of the solution and light excitation are also described.

Experimental Section

7-Hydroxyflavylium chloride was prepared according to a published procedure.[12] All other chemicals used were of analytical grade. The experiments were carried out in water at 25 °C. The pH of the solutions was adjusted by addition of $HClO_4$ (pH < 2) or buffer,[13] and measured by a Metrohm 713 pH meter. For ^{1}H NMR spectroscopy experiments 7-hydroxyflavylium chloride was dissolved in DCl (ca. 0.5 M). When required the pH was changed by addition of small aliquots of NaOD (1 M or 0.1 M). pH measurements were made in the NMR tube with an Ingold glass electrode, and the reported pH values, denoted with an asterisk, are direct readings without correction for the isotope effect.[14]

NMR spectroscopy[7, 8a] and flash photolysis[9a, 9b] experiments were performed as previously described. UV/Vis absorption and emission spectra were recorded on a Perkin–Elmer Lambda 6 spectrophotometer and a Perkin–Elmer LS 50 spectrofluorimeter, respectively. Photoexcitation in continuous irradiation experiments was performed using a medium-pressure mercury lamp and interference filters (Oriel) to isolate the excitation bands. The incident light intensity was measured by ferrioxalate actinometry.[15] The estimated error in quantum yield values is ±10%.

Results and Discussion

Equilibria in the dark: As shown in Scheme 1, in acidic and neutral aqueous solutions of synthetic flavylium ions it is possible to distinguish five forms: the flavylium cation ($\mathbf{A}H^+$); the quinoidal base (**A**), obtained by simple deprotonation of the flavylium cation [Eq. (1)]; the hemiacetal form (**B**), obtained by hydration of the flavylium cation [Eq. (2)]; the *cis*-chalcone form ($\mathbf{C_c}$), formed from the hemiacetal through a tautomeric process [Eq. (3)]; and the *trans*-chalcone form ($\mathbf{C_t}$), resulting from isomerization of *cis*-chalcone [Eq. (4)].

$$\mathbf{A}H^+ \overset{K_a}{\rightleftharpoons} \mathbf{A} + H^+ \quad (1)$$

$$\mathbf{A}H^+ \overset{K_h}{\rightleftharpoons} \mathbf{B} + H^+ \quad (2)$$

$$\mathbf{B} \overset{K_t}{\rightleftharpoons} \mathbf{C_c} \quad (3)$$

$$\mathbf{C_c} \overset{K_i}{\rightleftharpoons} \mathbf{C_t} \quad (4)$$

As shown previously[2, 8a] the molar fraction of the acidic form $\mathbf{A}H^+$ can be obtained from Equation (5), with K_a' given by Equation (6).

$$\frac{[\mathbf{A}H^+]}{C_0} = \alpha = \frac{[H^+]}{[H^+] + K_a'} \quad (5)$$

$$K_a' = K_a + K_h + K_h K_t + K_h K_t K_i \quad (6)$$

Equation (5) accounts for the complex equilibria described by Equations (1) to (4) in terms of a single acid–base equilibrium [Eq. (7)][8a] between the acidic species $\mathbf{A}H^+$ and a conjugate base **CB** having a concentration equal to the sum of the concentrations of the species **A**, **B**, $\mathbf{C_c}$, and $\mathbf{C_t}$, and molar fraction given by Equation (8).

$$\mathbf{A}H^+ \overset{K_a}{\rightleftharpoons} \mathbf{CB} + H^+ \quad (7)$$

$$\frac{[\mathbf{A}] + [\mathbf{B}] + [\mathbf{C_c}] + [\mathbf{C_t}]}{C_0} = \beta = \frac{K_a'}{[H^+] + K_a'} = 1 - \alpha \quad (8)$$

The individual expressions of the molar fractions of each component of **CB** can be easily calculated as shown in ref. [8a]. If the pH is sufficiently high to consider the system to be entirely in the **CB** form ($\beta = 1$), the relationships shown in Equation (9) apply.

$$\frac{[\mathbf{A}]}{C_0} = \frac{K_a}{K_a'}; \quad \frac{[\mathbf{B}]}{C_0} = \frac{K_h}{K_a'}; \quad \frac{[\mathbf{C_c}]}{C_0} = \frac{K_h K_t}{K_a'}; \quad \frac{[\mathbf{C_t}]}{C_0} = \frac{K_h K_t K_i}{K_a'} \quad (9)$$

The UV/Vis absorption spectra of dark-equilibrated aqueous solutions of the 7-hydroxyflavylium ion as a function of pH are shown in Figure 1. The spectral variations observed

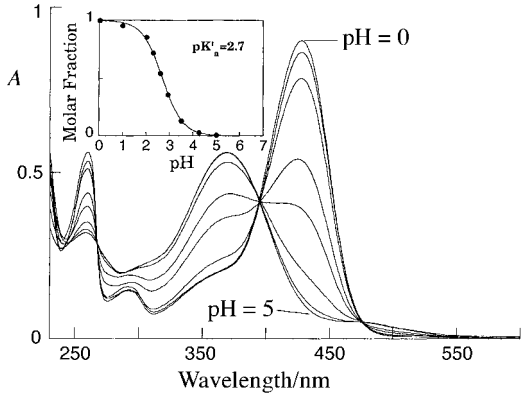

Figure 1. UV/Vis absorption spectra of dark-equilibrated aqueous solutions of the 7-hydroxyflavylium ion as a function of pH, from pH = 0 to pH = 5. Inset: molar fraction of $\mathbf{A}H^+$ as a function of pH.

are similar to those previously found for the 4′,7-dihydroxyflavylium and 4′-hydroxyflavylium ions. At pH ≤ 1.0 the predominant form is the flavylium cation $\mathbf{A}H^+$. The intensity of the $\mathbf{A}H^+$ band ($\lambda_{max} = 435$ nm) decreases with increasing pH, and two bands with maxima near 360 nm and 460 nm appear, assigned to *trans*-chalcone and quinoidal base, respectively.

The above results were confirmed by ^{1}H NMR experiments, where no hemiacetal (**B**) or *cis*-chalcone ($\mathbf{C_c}$) could be detected. The ^{1}H NMR spectrum of an acidic solution of 7-hydroxyflavylium chloride (pH* = 0.12) is shown in Figure 2a; the assignments are presented in Table 1. The spectrum is consistent with the existence of a sole species which, at this pH value, must be the flavylium cation, $\mathbf{A}H^+$. The assignments given in Table 1 were made on the basis of the following considerations:

1) The H atom at C-4′ is the only one expected to appear as a triplet with a relative integration of one proton; thus, the resonance at $\delta = 7.61$ must be assigned to it.

0947-6539/98/0410-2002 $ 17.50+.50/0 *Chem. Eur. J.* **1998**, *4*, No. 10

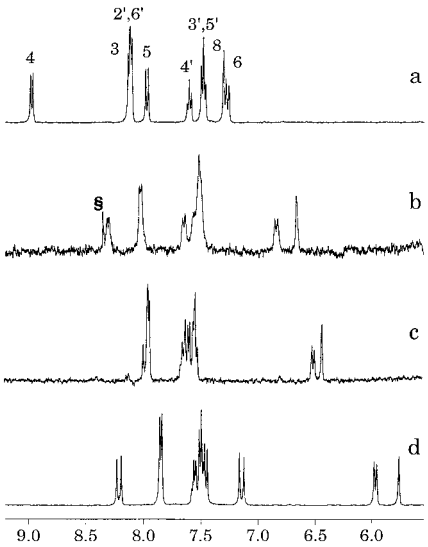

Figure 2. 400-MHz ^{1}H NMR spectra of 7-hydroxyflavylium chloride in D_2O at 27 °C: a) pH* = 0.12; b) same solution, after pH* jump to 7.3 and filtration; c) same solution as b) after ca. 24 h; d) pH* = 12.0. In spectrum b) the symbol § denotes an impurity.

Table 1. Chemical shifts (δ) and scalar couplings (J [Hz]) of some forms of 7-hydroxyflavylium chloride obtained by ^{1}H NMR in D_2O at 27 °C.

	$\mathbf{AH}^{+}$[a]		$\mathbf{A}$[b,c]	$\mathbf{C_t}$[b]		$\mathbf{C_t}^{2-}$[d]	
	δ	J	δ	δ	J	δ	J
2′-H + 6′-H	8.1[e]	–	8.02	7.9[e]	–	7.83	7.4
3′-H + 5′-H	7.48	7.8	7.5[e]	7.5[e]	–	7.48	7.5
4′-H	7.61	7.2	7.5[e]	7.62	7.3	7.54	–
3-H	8.1[e]	–	7.74[f]	7.5[e]	–	7.13	14.9
4-H	8.98	8.4	8.31[f]	7.9[e]	–	8.20	14.9
5-H	7.97	8.8	7.5[e]	7.5[e]	–	7.44	8.9
6-H	7.27	8.8	6.84	6.47	8.5	5.95	8.9
		2.0			–		–
8-H	7.31	–	6.66	6.39	2.0	5.75	1.8

[a] pH* = 0.12. [b] pH* = 7.3. [c] Coupling constants are not given due to low resolution. [d] pH* = 12.0. [e] Overlapped peaks. [f] Tentative assignment.

2) The resonance at 7.27 ppm appears as a doublet of doublets with very different scalar coupling constants (J = 8.8 and 2.0 Hz) and with integration of one H atom, which is consistent with the pattern expected for H-6.
3) Full assignment follows from COSY and NOESY spectra, the latter being necessary to distinguish between the resonances of H-3 and H-4.

When the yellow-orange solution (pH* = 0.12) is subjected to a pH jump to pH* = 7.3, a copious precipitate and a color change to red-orange are observed. After filtration, the ^{1}H NMR spectrum of the solution is consistent with the presence of a single species (Figure 2b). This spectrum evolves slowly (ca. 24 h at pH* = 7.3) into another one (Figure 2c), again characteristic of a single species, through a series of intermediate spectra showing peaks of both species. The final solution has an orange color. These results are consistent with the formation of the neutral quinoidal base **A** (which in part precipitates) as a consequence of the pH jump, followed by its rearrangement to *trans*-chalcone $\mathbf{C_t}$.

The assignment of the ^{1}H NMR spectra to the *trans* or *cis* isomer is usually made on the basis of the value of the coupling constant between H atoms 3 and 4.[7] In this case the attribution is not straightforward, owing to the overlap of these peaks with the signals of other H-atoms. The assignment of the spectrum in Figure 2c to *trans*-chalcone can, however, be made indirectly. Dissolving 7-hydroxyflavylium chloride in NaOD (0.01 M) gives a solution with the spectrum shown in Figure 2d. This spectrum can be attributed to the dibasic form of *trans*-chalcone ($\mathbf{C_t}^{2-}$); the complete assignment of this spectrum, given in Table 1, is based on the coupling constant from COSY and NOESY spectra, beginning with reasoning similar to that outlined above for the flavylium cation. Acidification of this solution to pH* < 6 is expected to give $\mathbf{C_t}$ and leads, in fact, to a spectrum identical to the one shown in Figure 2c. Assignments for **A** and $\mathbf{C_t}$ in Table 1 were made by comparison with the firm assignments made for the two other species.

The global acidity constant K_a' of 7-hydroxyflavylium was calculated from UV/Vis absorption spectra by measuring the molar fraction distribution of the $\mathbf{AH}^{+}$ species as a function of pH, as previously described.[8a] The results are shown in the inset of Figure 1, from which the value $pK_a' = 2.7$ was obtained.

Kinetic information from pH jump experiments: Kinetic information about the reactions reported in Scheme 1 can be obtained by displacing the system from equilibrium by means of a pH jump. pH jumps can be performed in both directions, starting from equilibrated solutions at pH 1 to high pH values, or vice versa. Figure 3 refers to a pH jump experiment from

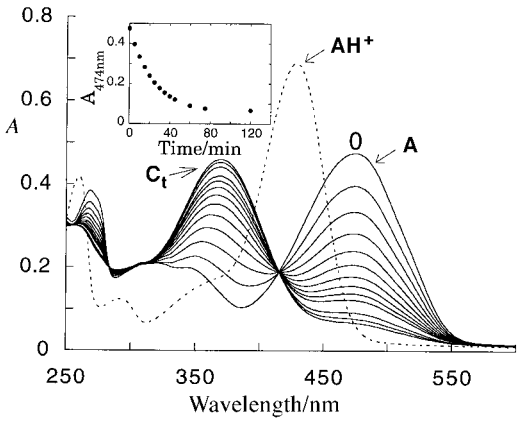

Figure 3. UV/Vis spectral variations in the dark for the 7-hydroxyflavylium ion (2.5×10^{-5} M) upon a pH jump from pH = 1.0 to pH = 6.0. The inset shows the change in absorbance at λ = 474 nm (maximum of the quinoidal base **A**) as a function of time.

pH 1.0 to pH 6.0. The results obtained show the existence of two reactions occurring on different time scales, as was previously observed for 4′,7-dihydroxyflavylium.[9a, 9b] As shown by the absorption spectrum obtained immediately after the pH jump, the first reaction is the deprotonation of the flavylium cation ($\mathbf{AH}^{+}$) to give the quinoidal base (**A**). This reaction is too fast to be followed by a stopped-flow apparatus. The ratio between the concentrations of $\mathbf{AH}^{+}$ and **A** after the pH jump is dependent only on the acidity constant K_a. The second process, which is slow enough to be monitored

by spectrophotometric analysis, is the partial conversion of **A** into the *trans*-chalcone ($\mathbf{C_t}$). At pH 6.0 the only species absorbing at 460 nm is **A**; consequently, the ratio between the final absorbance and the initial absorbance after this second process is equal to the molar fraction of this species at equilibrium with $\mathbf{C_t}$. From the data of Figure 3, the molar fraction of **A** when $\beta = 1$ is calculated to be 0.14, which allows us to obtain $K_a = 2.8 \times 10^{-4}$ and $K_h K_t K_i = 1.7 \times 10^{-3}$ from Equation (9).

Kinetic analysis of the slow process shows first-order behavior with a rate constant which depends on pH but not on the direction of the pH jump (Figure 4). Similar behavior

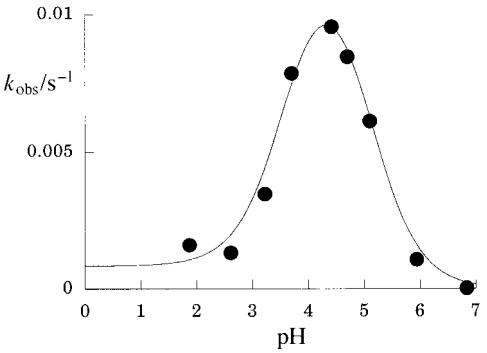

Figure 4. pH dependence of the first-order rate constant of the slowest process observed upon a pH jump carried out on aqueous solutions of 7-hydroxyflavylium ion. The solid line is a fit to the experimental data based on Equation (11).

was recently described for the parent compound 4′,7-dihydroxyflavylium.[9b] As in that case, the reactions occurring in the system can be represented by Equations (1) and (10), where **X** is the intermediate state consisting of **B** and $\mathbf{C_c}$ in rapid equilibrium. Because **X** does not accumulate, its formation must be slower than its disappearance. This is possible if formation of $\mathbf{C_t}$ from $\mathbf{A}H^+$ and **A** is controlled by the hydration reaction that leads to **B** and the back-formation of $\mathbf{A}H^+$ and **A** from $\mathbf{C_t}$ by *trans*–*cis* isomerization (Scheme 1). In other words, $k_h \ll k_{-h}[H^+]$ and $k_{-i} \ll k_i$. A kinetic treatment, based on the steady-state approximation for the intermediate species **X** and considering that the equilibrium in Equation (1) is by far the fastest process of the system, leads to Equation (11).[9b]

$$\mathbf{A}H^+ \overset{K_a}{\rightleftharpoons} \mathbf{A} + H^+ \quad (1)$$

$$\mathbf{A}H^+ \underset{k_h[H^+]}{\overset{k_h}{\rightleftharpoons}} \mathbf{X} \underset{k_{-i}}{\overset{k_i}{\rightleftharpoons}} \mathbf{C_t} \quad (10)$$

$$k_{obs} = \frac{[H^+]}{[H^+] + K_a} \cdot \frac{k_i k_h}{k_i + k_{-h}[H^+]} + \frac{k_{-i} k_{-h}[H^+]}{k_i + k_{-h}[H^+]} \quad (11)$$

Representation of Equation (11) as a function of pH yields a bell-shaped curve (Figure 4) from which the rate constants can in principle be evaluated by a fitting procedure. However, since $k_h \ll k_{-h}[H^+]$ and $k_{-i} \ll k_i$, only the rate constants k_{-i} and k_h of the rate-determining steps affect the shape of the curve and can therefore be obtained. Their values are shown in Table 2, where the corresponding values previously obtained[6, 9, 11] for the 4′,7-dihydroxyflavylium and 4′-hydroxyflavylium ions are also shown for comparison purposes.

Table 2. Thermodynamic and kinetic constants.[a]

Compound	7-OH[b]	4′-7-diOH[c]	4′-OH[d]
K'_a	$10^{-2.7}$	$10^{-3.05}$	$10^{-1.9}$[e]
K_a	$10^{-3.55}$	10^{-4}	$10^{-5.5}$
K_h	8×10^{-6}	1.4×10^{-6}	3.6×10^{-6}
K_i	5×10^{2}	1.4×10^{3}	3.5×10^{3}
k_h	$0.48\ s^{-1}M^{-1}$	$1.8 \times 10^{-2}\ s^{-1}M^{-1}$	$8.9 \times 10^{-2}\ s^{-1}M^{-1}$
k_{-h}[f]	$3 \times 10^{4}\ s^{-1}M^{-1}$	$1.3 \times 10^{4}\ s^{-1}M^{-1}$	$2.5 \times 10^{4}\ s^{-1}M^{-1}$
k_i	$0.57\ s^{-1}$[f]	$0.26\ s^{-1}$[f]	$3.7 \times 10^{-5}\ s^{-1}$
k_{-i}	$8.3 \times 10^{-4} s^{-1}$	$1.8 \times 10^{-4}\ s^{-1}$	$\approx 10^{-8}\ s^{-1}$

[a] Measured by means of pH jump techniques at 25 °C unless otherwise noted. [b] This work. [c] Ref. [9b]. [d] Refs. [6] and [11]. [e] Value reported at 60 °C. [f] Flash photolysis.

Photochemical experiments:

Continuous irradiation: The spectral changes observed upon steady-state irradiation of solutions of *trans*-chalcone with 365 nm light at pH 2.75 are shown in Figure 5. The most

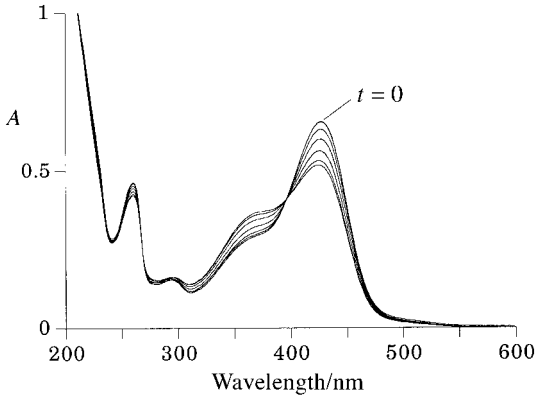

Figure 5. Steady-state irradiation of the compound 7-hydroxyflavylium at $\lambda = 365$ nm and pH 2.75; the curves refer to irradiation times from 0 to 30 minutes, when a photostationary state is reached.

relevant aspect of these results, when compared with those obtained from 4′,7-dihydroxyflavylium[9a, 9b] and 4′-hydroxyflavylium,[6, 11] is the low yield of the net conversion. This behavior is at least in part due to the fact that in the case of 7-hydroxyflavylium the thermal back-reaction that restores *trans*-chalcone is faster than in the other cases (for more details, see below). The initial quantum yield of formation of flavylium cation/quinoidal base, $\mathbf{A}/\mathbf{A}H^+$, calculated on the basis of the total light absorbed by the system, changes on changing the pH of the solution, as shown in Figure 6. The maximum value for the observed quantum yield is obtained at pH ≈ 3. It should be noted that the decrease observed for low pH values is an artefact due to the decrease in the molar fraction of *trans*-chalcone as the pH becomes lower than 3. The important point is that the observed quantum yield decreases sharply at high pH values where the molar fraction of *trans*-chalcone reaches its maximum value. As we will see below, this result is due to the fact that at high pH values the transformation of $\mathbf{C_t}$ to $\mathbf{A}H^+$ is prevented, favoring the reversion of $\mathbf{C_c}$ into $\mathbf{C_t}$.

It is worth noting that no significant spectral variation was observed upon 1-hour irradiation of solutions of 7-hydroxy-

0947-6539/98/0410-2004 $ 17.50+.50/0 *Chem. Eur. J.* **1998**, *4*, No. 10

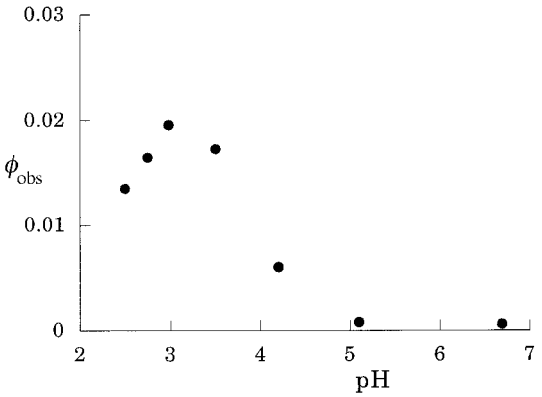

Figure 6. Quantum yield of formation of quinoidal base **A** and flavylium cation $\mathbf{AH}^+$ calculated on the basis of the total light absorbed by the system after 0.5 min of irradiation, as a function of the pH of the solution.

flavylium at pH 1.0, showing that the flavylium cation is photochemically stable.

Fluorescence emission: Fluorescence was observed upon excitation of the three forms of 7-hydroxyflavylium ion $\mathbf{AH}^+$, **A**, and $\mathbf{C_t}$ (Figure 7). The fluorescence spectrum

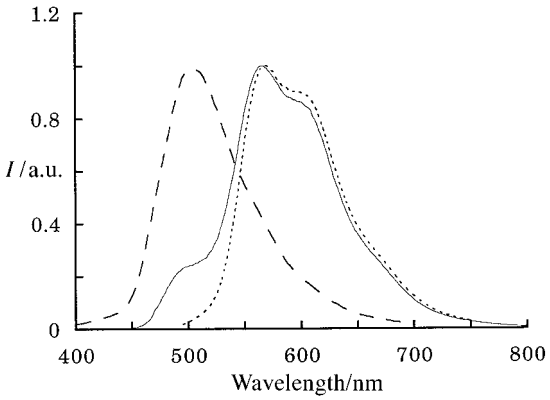

Figure 7. Fluorescence spectra of the 7-hydroxyflavylium ion: dark equilibrated solution at pH = 5.0, λ_{exc} = 370 nm (dashed line); immediately after a pH jump from pH = 1.0 to 6.0, λ_{exc} = 470 nm (dotted line); dark-equilibrated solution at pH = 1.0, λ_{exc} = 470 nm (solid line).

recorded at pH = 1, where $\mathbf{AH}^+$ is the sole species present in solution, shows a band that is identical to that observed by selective excitation (λ_{exc} = 470 nm) of **A** at pH = 6, except for the shoulder around 500 nm. The excitation spectrum of the solution at pH = 1.0 and λ_{em} = 600 nm matches the absorption spectrum of $\mathbf{AH}^+$, and the excitation spectrum of the emission of **A** (pH = 6.0 and λ_{em} = 600 nm) is coincident with the absorption spectrum of **A**. The results show that at pH = 1.0, in spite of the fact that we are exciting $\mathbf{AH}^+$, most of the emission is due to the excited state of **A**. This behavior, already described for other flavylium salts containing hydroxyl groups in the 7-position (namely 3,4′-dimethoxy-7-hydroxyflavylium,[8a] 4′,7-dihydroxyflavylium, and 4-methyl-7-hydroxyflavylium[16]), is due to the adiabatic deprotonation of the excited state of $\mathbf{AH}^+$.

The emission from $\mathbf{C_t}$, also shown in Figure 7, shows a large Stokes shift with respect to the absorption band indicating that the geometry of the excited state is different from that of the ground state. This behavior was found in other compounds exhibiting a *cis–trans* isomerization[17] and is in agreement with the photochemical behavior of this species (see below).

Flash photolysis: As mentioned above, pH jump experiments can give the rate constants corresponding only to the rate-determining step in each direction, that is, the *trans*→*cis* isomerization and the hydration reaction $\mathbf{AH}^+ \rightarrow \mathbf{B}$. Fortunately, the pH jump technique can be complemented by flash photolysis, where the equilibrium is displaced by means of a pulse of light.[9]

Dark-equilibrated solutions of 7-hydroxyflavylium chloride were irradiated with a flash lamp (pulse width of a few milliseconds), and the changes in absorbance were monitored as a function of time. In Figure 8 the traces obtained at 460 nm

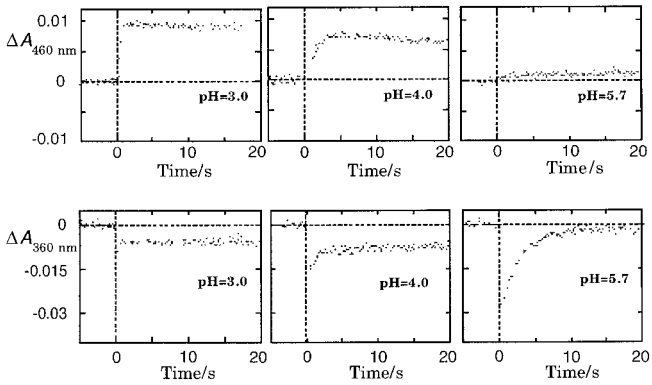

Figure 8. Changes in absorbance at λ = 460 and 360 nm observed after flash excitation of 7-hydroxyflavylium solutions at three representative pH values.

(absorption maximum of **A**) and 360 nm (absorption maximum of $\mathbf{C_t}$) are shown for three representative pH values, 3.0, 4.0, and 5.7. As in the case of 4′,7-dihydroxyflavylium,[9a, 9b] the absorbance decay traces clearly show the presence of three consecutive kinetic processes. The first one occurs within the flash and is too fast to be monitored with our apparatus. It can be assigned to the reaction of $\mathbf{C_t}$ to give $\mathbf{C_c}$ in equilibrium with hemiacetal **B**. The second process ends within a few seconds, whereas the third process (not shown in Figure 8), falls into the time domain of minutes and completely restores the initial absorbance (before irradiation). Differential time-resolved spectra were obtained from traces such as those reported in Figure 8 by plotting the difference between the initial absorbance and the absorbance at various time delays (Figure 9). Inspection of Figure 9 shows that on a time scale of seconds the disappearance of $\mathbf{C_t}$ (bleaching at 360–380 nm) leads to formation (through the $\mathbf{C_c}$ isomer) of **A** and $\mathbf{AH}^+$ (increase of absorbance in the visible region). The traces recorded at 460 nm (Figure 8) show that the formation of **A** and $\mathbf{AH}^+$ occurs by a first-order process that becomes faster and more efficient with decreasing pH. The same rate constant is obtained from the parallel recovery of absorbance at 360 nm. These results show that the *cis*-chalcone formed by light excitation is an unstable species which disappears by a pH-controlled forward reaction to give quinoidal base and

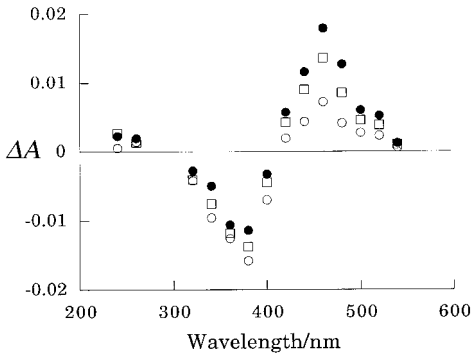

Figure 9. Differential time-resolved UV/Vis spectra for 7-hydroxyflavylium solutions after a flash excitation at pH 4.25: 0.5 (○), 1 (□), 3 (●) seconds after the flash.

flavylium cation, and by the back-reaction yielding *trans*-chalcone. Therefore, the flash photolysis experiments yield information on the fast processes (dehydration and *cis* →*trans* isomerization) not accessible to the pH jump technique. Following a procedure described previously,[9b] the rate constants $k_{-h}[H^+]$ and k_i have been evaluated from the absorbance changes (Table 2).

Substituent effects: With the data shown in Table 2, the energy-level diagram shown in Figure 10 can be drawn for the 7-hydroxyflavylium ion. The energy-level diagrams for the previously investigated 4′-hydroxyflavylium[11] and 4′,7-dihydroxyflavylium[9a, 9b] ions are also shown in Figure 10 for comparison purposes.

The effect of substituents on the photochromic behavior of the three flavylium ions can now be discussed. As is evident from Figure 10, in all cases $\mathbf{A}H^+$ is the thermodynamically stable form in acidic medium, but on increasing pH it becomes less stable than $\mathbf{C_t}$ and, at high pH, also than $\mathbf{C_c}$. The most noticeable difference among the three compounds concerns the value of the rate constant of the *cis* →*trans* isomerization reaction (k_i) which for the 4′-OH derivative is several orders of magnitude lower than for the other two compounds (Table 2). Because of such a low rate constant, for the 4′-OH derivative the *cis* isomer formed upon light excitation in acidic solutions is quantitatively converted by the much faster reaction (rate constant $k_{-h}[H^+]$) of its tautomeric form **B** to give the species $\mathbf{A}H^+$ (in fast equilibrium with **A**), which can be indefinitely stored. The reversion of $\mathbf{A}H^+$ and **A** to $\mathbf{C_t}$ (via **B** and $\mathbf{C_c}$), however, can be encouraged by raising the temperature and/or pH of the solution, as well as by means of the photochemical isomerization of $\mathbf{C_c}$. As discussed elsewhere, such behavior is suitable for optical memory devices with nondestructive readout capacity through a *write-lock-read-unlock-erase* cycle.[10] Such a possibility, however, is precluded for the 7-OH and 4′,7-OH derivatives because k_i is much larger; therefore, i) the rate of the *cis* →*trans* isomerization reaction competes with the forward reaction leading from $\mathbf{C_c}$ to $\mathbf{A}H^+$, and ii) $\mathbf{A}H^+$ and **A** revert rapidly to $\mathbf{C_c}$ and $\mathbf{C_t}$, except at very low pH values.

Differences are also noticeable in the rate constants of the various processes for the 7-OH and 4′,7-OH derivatives (Table 2). All the rate constants are higher for the 7-OH

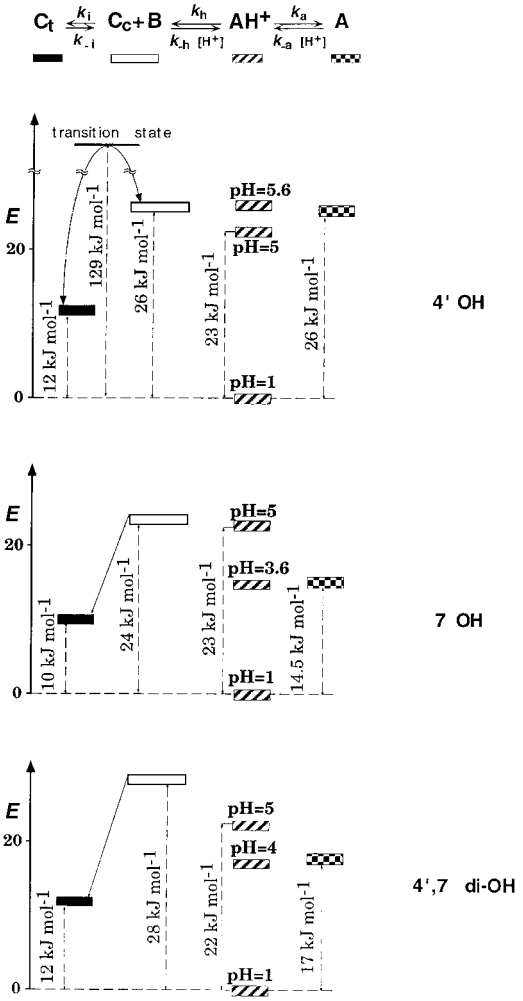

Figure 10. Energy-level diagrams for the species involved in the transformation of 7-hydroxyflavylium ion and of the previously investigated 4′-hydroxyflavylium[11] and 4′,7-dihydroxyflavylium[9a, 9b] ions.

derivative, but it should be noted that whereas k_{-h} is less than 3 times larger, k_h is more than 20 times larger. It follows that at any given pH value the $\mathbf{A}H^+$ species is less stable (relative to **B**) in the 7-OH derivative. Therefore in the 7-OH derivative the time for which the colored species can be transiently observed in flash experiments is shorter, and the amount of colored species present at the photostationary state in continuous irradiation experiments is smaller.

Conclusions

We have investigated the processes which occur in aqueous solutions of the 7-hydroxyflavylium ion during pH jump and continuous and flash photolysis experiments. The rate constants and equilibrium constants of the various structural transformations have been obtained and compared with those previously reported for the 4′-hydroxyflavylium and 4′,7-dihydroxyflavylium ions. The various forms of these compounds are related by interconverting processes in a manner reminiscent of a system of connecting vessels. Using such a hydraulic analogy, the behavior of an aqueous solution of

0947-6539/98/0410-2006 $ 17.50+.50/0 *Chem. Eur. J.* **1998**, *4*, No. 10

Efficient Homogeneous Hydrosilylation of Olefins by Use of Complexes of Pt^0 with Selected Electron-Deficient Olefins as Ligands

Pascal Steffanut, John A. Osborn,* Andre DeCian, and Jean Fisher*

Abstract: A family of complexes of general formula $[Pt(\eta^2\text{-}Ol_E)\{(\eta^4\text{-}CH_2{=}CHSiMe_2)_2O\}]$, where Ol_E is a di-, tri- or tetrasubstituted electron-deficient olefin such as fumaronitrile, diethylfumarate, tetracyanoethylene, ethylenetetracarboxylate, a naphthoquinone or dihydronaphthoquinone, were synthesised from the Karstedt catalyst solution containing $[Pt_2(CH_2{=}CHSiMe_2)_2O)_3]$ (**1**). The structures of these complexes were examined by ^1H, ^{13}C and ^{195}Pt NMR spectroscopy. The X-ray crystallographic structure of $[Pt(\eta^2\text{-MeNQ})\{(\eta^4\text{-}CH_2{=}CHSiMe_2)_2O\}]$ (MeNQ = methylnaphthoquinone) was determined; the MeNQ ligand is bound to Pt by a η^2-olefin interaction. Certain of these complexes, particularly the naphthoquinone and dihydronaphthoquinone derivatives, were found to catalyse very efficiently the hydrosilylation of a variety of olefins. Tests in the presence of Hg, dibenzo[*a,e*]cyclooctatetraene or molecular oxygen indicated that the catalytic process was homogeneous in nature. The addition of excess Ol_E to the catalyst solutions greatly extended the lifetime and productivity of these catalysts, which were more efficient both in rate and overall product yield than the original Karstedt catalyst solution. Spectroscopic studies lead us to propose that the stabilising ligand Ol_E remains bound to Pt throughout the catalytic cycle; this results in increased stability and high catalytic activity.

Keywords: alkene complexes · heterogeneous catalysis · homogeneous catalysis · hydrosilylations · naphthoquinones · platinum

Introduction

Hydrosilylation of olefins is one of the most important reactions in silicon chemistry (Scheme 1).[1] Among the numerous catalysts for this reaction, the most efficient are

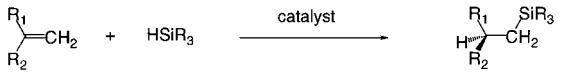

Scheme 1. The catalytic hydrosilylation of olefins.

those which involve platinum complexes, particularly the original[2] Speier catalyst, H_2PtCl_6, and the second-generation[3] Karstedt catalyst, which are presently those largely used in commercial processes. However, the detailed mechanism of the catalytic process using these Pt-based systems remains uncertain since both homogeneous and heterogeneous catalytic behaviour have been invoked. Indeed, the Pt precursors are intrinsically unstable under hydrosilylation conditions and metal-containing particles are readily formed in solution. Such observations, inter alia, have led Lewis and co-workers to suggest that colloids may be responsible for the catalytic activity.[4]

We report here the synthesis of a family of molecular platinum(0) compounds for the hydrosilylation of olefins and studies of their catalytic activity. These catalysts are more active and more stable than the classical Karstedt catalyst systems under identical conditions and evidence is presented indicating that their catalytic action is homogeneous in nature.

Initial observations: The Karstedt catalyst solution is formed by the reaction of the diene $(CH_2{=}CHSiMe_2)_2O$ (hereafter dvtms) with H_2PtCl_6. The active catalyst precursor is probably the Pt^0 complex, $[Pt_2(CH_2{=}CHSiMe_2)_2O)_3]$ (**1**), which is preponderant in such solutions and has been characterised by an X-ray structural determination (Figure 1).[5] We note that the Karstedt catalyst solution normally used also contains an excess of dvtms.

[*] Prof. J. A. Osborn, Dr. P. Steffanut
Laboratoire de Chimie des Métaux de Transition et Catalyse
Université Louis Pasteur, Institut Le Bel
URA 424 CNRS, 4 rue Blaise Pascal
F-67070 Strasbourg Cedex (France)
Fax: (+33) 38-841-6171
E-mail: osborn@chimie.u-strasbg.fr
Prof. J. Fisher, A. Decian
Laboratoire de Cristallochimie et de Chimie Structurale
Université Louis Pasteur, Institut Le Bel
URA 424 CNRS, 4 rue Blaise Pascal
F-67070 Strasbourg Cedex (France)
Fax: (+33) 38-841-5363
E-mail: fischer@chimie.u-strasbg.fr

0947-6539/98/0410-2008 $ 17.50+.50/0 *Chem. Eur. J.* **1998**, *4*, No. 10

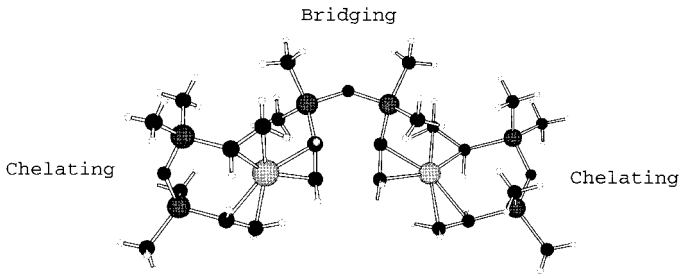

Figure 1. Chem3D representation of $[Pt_2(dvtms)_3]$.

We initially studied the Karstedt catalyst (6×10^{-6} mol) using the substrates allyl alcohol (3×10^{-3} mol) and Et_3SiH (3×10^{-3} mol) in hexane (30 mL) at 72 °C. It was observed that if the silane was added dropwise to a prepared catalyst/olefin solution, the rate of addition strongly influenced the overall yield of hydrosilylation product. Hence if the rate of dropwise addition of Et_3SiH was increased from 1.5×10^{-4} mol min^{-1} (i.e., added over 20 min) to 3×10^{-4} mol min^{-1} (added over 10 min), the final yield of product decreased from ca. 37% to 20%, no further reaction taking place after one hour. However if the initial olefin concentration was doubled (6×10^{-3} mol), the corresponding yields were 74% and 62% respectively. Similar effects were observed using styrene as substrate. Further, it was noticed that the more rapidly the silane was added, the earlier a black precipitate appeared in the solution. These observations indicated that the catalyst appeared to be less stable as the concentration of the silane increased but this effect could be compensated in part by the presence of higher concentrations of olefin substrate.

Experiments were then carried out in which the silane was added initially to the catalyst solution and the olefin added after a certain delay, *t*. Under the same standard conditions described above, a) when $t = 5$ min, the initial rate was ca. 12 equiv min^{-1} with a total yield of 48%, b) with $t = 10$ min the rate was 5 equiv min^{-1} and the yield 40%, and c) with $t =$ 30 min. the values were ca. 3.5 equiv min^{-1} and 16%. Again we observed that the greater the value of *t*, the earlier the deposition of black material took place. If colloid particles of an optimum size were necessary for high activity,[4] then it might be anticipated that a correlation of the highest activity would occur with some optimum value of the contact time *t*, where $t > 0$. In fact we see that the initial rate of hydrosilylation always decreased with an increase in *t* and the colloids formed appeared to be much less active (if active at all) than the initial homogeneous solutions. We attempted to stabilise the colloids formed using three micelle-forming amphiphiles (sodium dodecylsulfonate (SDS), *N*-cetyl-*N,N,N*-trimethylammonium bromide and polyethyleneglycol hexadecyl ether), but the catalytic activity was either unaffected (SDS) or diminished.

We therefore redirected our attention towards the stabilisation of the molecular Pt species in solution. It is well known that phosphine complexes,[6] such as $[Pt(SiR_3)(\mu\text{-}H)(R_3P)]_2$, $[Pt(PR_3)\{(\eta^4\text{-}CH_2{=}CHSiMe_2)_2O\}]$, are less active than the Karstedt catalyst but are stable under hydrosilylation conditions at ambient temperatures. We found that when the complexes $[Pt(PR_3)\{(\eta^4\text{-}CH_2{=}CHSiMe_2)_2O\}]$ (with R = alkyl, aryl, or substituted aryl) were used as catalysts for the reaction of $HSiEt_3$ with $Et_3Si(CH{=}CH_2)$, after an induction period of ca. 1 h, the reactivity of the catalysts at 30 °C decreased in the order: R = *p*-fluorophenyl > phenyl > *m*-tolyl > cyclohexyl > *tert*-butyl. Although this trend may be a result of several factors, the catalysts with the more electron-attracting phosphines were the most efficient. We surmised that with even stronger π-acid ligands, catalysts possessing greater activity might be obtained, and therefore we synthesised Pt^0 complexes of electron-deficient olefins with this in mind.

Results and Discussion

Synthesis of $[Pt(\eta^2\text{-}Ol_E)\{(\eta^4\text{-}CH_2{=}CHSiMe_2)_2O\}]$ complexes (Ol_E = electron-deficient olefin): It had been previously reported[5] that $[Pt_2\{((CH_2{=}CH)SiMe_2)_2O\}_3]$ (**1**) reacts with maleic anhydride to form $[Pt(\eta^4\text{-dvtms})(\eta^2\text{-maleic anhydride})]$. Spectroscopic data indicated that the complex possessed a monomeric structure similar to that found for $[Pt(\eta^4\text{-1,5 hexadiene})(\eta^2\text{-maleic anhydride})]$, where an X-ray determination showed all three olefin groups coordinated to Pt in a nearly coplanar fashion.[7] The complexes $[Pt(\eta^2\text{-}C_2H_4)_2(\eta^2\text{-}C_2F_4)]$[8] and the recently described dimethylfumarate and dimethylmaleate[9] complexes have analogous structures. Interestingly, the fumarate and maleate complexes of Pt^0 were synthesised in studies with the objective of inhibiting the Pt-catalysed hydrosilylation process. We shall discuss this point later.

Using an adaptation of the reported procedure,[5] we synthesised complexes of the type $[Pt(\eta^2\text{-}Ol_E)\{(\eta^4\text{-}CH_2{=}CHSiMe_2)_2O\}]$ (Figure 2) by replacement of the bridging siloxane of $[Pt_2(CH_2{=}CHSiMe_2)_2O)_3]$ by Ol_E. The elec-

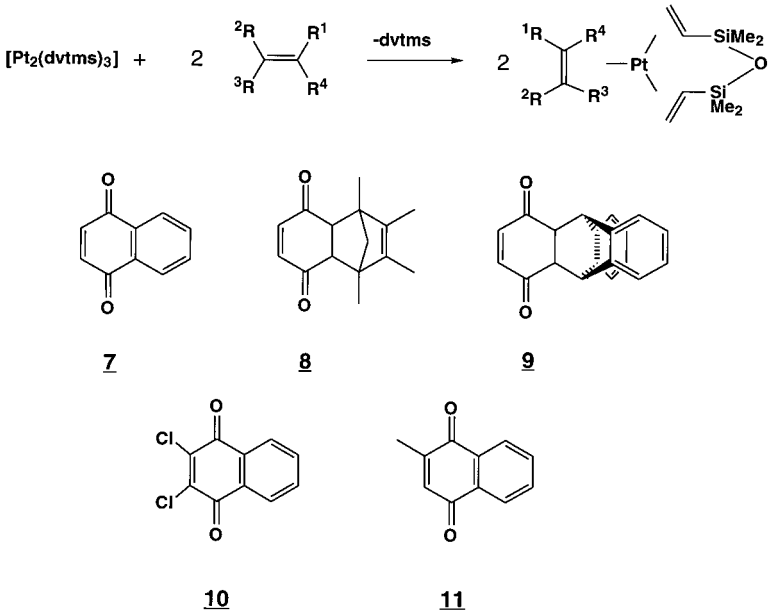

Figure 2. Substitution of $[Pt_2(dvtms)_3]$ by electrophilic olefins. The naphthoquinone ligands used and the numbers of the corresponding complexes **7**–**11** are also shown.

  0947-6539/98/0410-2009 $ 17.50+.25/0

tron-withdrawing substituents, E, on the olefins were aryl, CN, COR or COOR. Several naphthoquinone and dihydronaphthoquinone complexes were also prepared, which we label collectively as NQ′ complexes.

In general, slightly less than one equivalent of Ol_E was added to a toluene or hexane solution containing **1** at 20 °C to yield the desired products as colourless (or yellow for the NQ′ complexes) microcrystalline solids. We were unable to isolate complexes of the monosubstituted olefins styrene, vinyl acetate, ethylacrylate or allyl alcohol although the styrene derivative has previously been detected in solution by ^{195}Pt NMR.[10]

The complexes [Pt(η^2-Ol_E){(η^4-CH_2=$CHSiMe_2$)$_2$O}] **2**–**11** were obtained with *trans*-disubstituted olefins such as fumaronitrile (**2**), diethylfumarate (**3**) or *trans*-(PhCO)CH=CH-(COPh) (**4**); tetrasubstituted olefins $(EtOOC)_2C$=$C(COOEt)_2$ (**5**) or $(NC)_2C$=$C(CN)_2$ (**6**); and the NQ′ type ligands, naphthoquinone (NQ) (**7**); 1,2,3,4-tetramethyl-4*a*,8*a*-dihydro-*endo*-1,4-methylmethanonaphthalene-5,8-dione (TND) (**8**), 9,10-dihydro-9,10-*ortho*-benzenoanthracene-1,4-dione (BAD) (**9**), dichloronaphthoquinone (DCNQ) (**10**) or methylnaphthoquinone (MeNQ) (**11**). In addition the complex [Pt(η^2-norbornene)$_2$(η^2-(MeNQ)] (**12**) was prepared for comparative purposes. Details can be found in the Experimental Section.

Structures of the [Pt(η^2-Ol_E){(η^4-CH_2=$CHSiMe_2$)$_2$O}] complexes 2–11: Crystals of the methylnaphthoquinone complex **11** were obtained by slow evaporation of a saturated hexane solution and were analysed by X-ray diffraction methods. The structure is monoclinic with a $P2_1/n$ space group.[11] The detailed structure is shown in Figure 3 and the crystallographic data presented in Table 1.

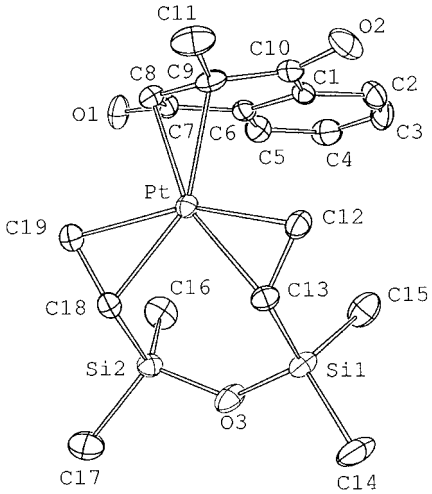

Figure 3. ORTEP plot of one molecule of **11** showing the labelling scheme used. Ellipsoids are scaled to enclose 50% of the electronic density. Hydrogen atoms are omitted.

The MeNQ ligand is bound solely by its olefinic double bond, leading to a closely trigonal coordination arrangement about the Pt atom as found for the other known structures of this type.[7] The electron-deficient olefin group is rotated somewhat out of the trigonal plane by an angle Θ, where Θ in this case is 17.8 ± 1.1°. In contrast, in the benzoquinone complex [Pt(1,5-cyclooctadiene)(η^4-ditertiobutylbenzoquinone),[8] both olefinic bonds of the quinone were found to be coordinated to Pt^0. The other notable feature of **11** is the chair conformation adopted by the $(CH_2$=$CHSiMe_2)_2O$ ligand, which leads to the axial–equatorial disposition of the CH_3 groups on the Si atoms. Similar observations have been made for the phosphine derivative, [Pt{(η-CH_2=$CHSiMe_2)_2O$}(PR_3)].[6] The significant bond distances and angles are presented in Table 2.

Table 1. X-ray crystallographic data for **11**.

formula	$C_{19}H_{26}O_3Si_2Pt \cdot H_2O$
molecular weight	571.69
crystal system	monoclinic
space group	$P2_1/n$
a (Å)	9.725(3)
b (Å)	10.426(3)
c (Å)	21.348(6)
β (°)	102.76(2)
V (Å^3)	2111(2)
Z	4
colour	yellow
crystal dim (mm)	$0.30 \cdot 0.24 \cdot 0.20$
ρ_{calcd} (g cm^{-3})	1.80
F000	1120
μ (mm^{-1})	6.846
trans. min and max	0.6990/1.0000
T (K)	294
λ (Å)	0.71073
radiation	$Mo_{K\alpha}$ graphite-monochromated
diffractometer	Enraf–Nonius CAD4
scan mode	$\theta/2\theta$
hkl limits	0,12/ − 13,13/ − 26,27
θ limits (°)	2.5/26.98
no. of data meas.	9738
no. of data with $I > 3\sigma(I)$	3480
weighting scheme	$4F_o^2/(\sigma^2(F_o^2) + 0.0025\,F_o^4)$
no. of variables	235
R	0.033
R_w	0.042
GOF	1.053
largest peak in final difference (e Å^{-3})	1.312

Table 2. Selected bond lengths [Å]and angles [°] for **11**.

Pt–C(8)	2.162	Pt–C(12)	2.179	C(12)–C(13)	1.35
Pt–C(9)	2.174	Pt–C(13)	2.204	C(8)-Pt-C(9)	37.6
Pt–C(18)	2.231	C(8)–C(9)	1.40	C(12)-Pt-C(13)	35.9
Pt–C(19)	2.205	C(18)–C(19)	1.37	C(18)-Pt-C(19)	36.0

The ^{1}H NMR data were consistent with the stoichiometry proposed for the complexes. The CH_3 groups on the Si atoms of the $(CH_2$=$CHSiMe_2)_2O$ ligand ($\delta \approx 1$ to -2) provided further information concerning the structures in solution. If the solid-state structure found for **11** were maintained and nonfluxional in solution, four different CH_3 resonances should be observed for all compounds if $\Theta > 0$. This was observed for complexes **2**, **4**, **5** and **6**. Since the diastereotopic CH_3 groups on each Si atom are not equilibrated, ready dissociation of the olefin groups of the dvtms ligand by a sequential arm-off mechanism can be excluded. This is the only mechanism that

0947-6539/98/0410-2010 $ 17.50+.50/0 *Chem. Eur. J.* **1998**, *4*, No. 10

would allow the Pt^0, which is bound to the *re* face of one diene olefinic bond and to the *si* face of the other, to gain access to the opposite faces of the diolefin. However, any rapid cyclohexane-type conformational changes of the dvtms ligand will not be observed since these would leave the CH_3 groups distinct. In the tetrasubstituted olefin complexes **5** and **6**, the presence of four CH_3 resonances indicated that the olefin must be bound rigidly at a definite angle Θ. Although a similar structure (with $\Theta > 0$) might be anticipated for **2** and **4** in solution, the ^1H NMR data cannot exclude an in-plane coordination and/or a rotational motion of the olefin since no differences in the $Si{-}CH_3$ spectrum would be observable. However in **4** the vinylic protons of the *trans*-dibenzoylethylene ligand exhibited a single resonance showing a $^2J(Pt,H)$ coupling of 60 Hz. Dissociation of the electron-deficient olefin cannot therefore be occurring readily, but facile rotation about the olefin axis is probably taking place.

The ^1H NMR spectrum of the NQ′ complexes **7**–**10** showed only two $Si{-}CH_3$ resonances; this can either be consistent with the solid-state structure (with $\Theta > 0$) found for **11** in which rapid olefin rotation was occurring, or a trigonal structure with $\Theta = 0$. As expected for **11**, the four $Si{-}CH_3$ resonances were distinct and coupling of ^{195}Pt with both the vinyl proton ($^2J(Pt,H) = 48$ Hz) and the methyl ($^3J(Pt,H) = 30$ Hz) on the MeNQ was observed. Again, no rapid dissociation of the MeNQ ligand can be taking place. Finally, other ^{195}Pt and ^{29}Si NMR data are given below the following section on catalysis.

Catalytic studies: The relative efficiencies of these Pt^0 complexes as hydrosilylation catalysts were compared by means of a standard reaction of $Me_3SiCH{=}CH_2$ with Et_3SiH. This reaction can also serve as a model for the cross-linking reaction used in an industrial siloxane polymer synthesis. The catalytic reactions were carried out with 30 mL of deoxygenated hexane solutions of $Me_3SiCH{=}CH_2$ (0.30 mol L^{-1}, 1000 equiv) and Et_3SiH (0.15 mol L^{-1}, 500 equiv) to which 6×10^{-6} mol of the given platinum complex was immediately added and stirred at 30 °C for 2 h. It is noteworthy that, unlike in conventional Karstedt procedures, dropwise addition of the silane was not necessary when using these catalysts. No induction period was observed and clean formation of $Me_3SiCH_2CH_2SiEt_3$ occurred with no by-products being detected by GC or NMR. The catalytic activities of the complexes **2**, **5**, **6** are compared in Figure 4 and the more active NQ′ complexes **7**, **8**, **10** and **11** in Figure 5. All reactions went to completion, the methylnaphthoquinone complex proving to be the most active.

The efficiency of these catalysts was compared with that of the Karstedt system by using equivalent Pt concentrations and measuring the time ($t_{1/2}$) needed to yield 50% of product (Table 3). It can be seen that that the NQ′ catalysts were all more active than the Karstedt catalyst solution and, moreover, no colour changes in the solution occurred during the catalytic process. The Karstedt catalyst solutions, on the other hand, quickly turned dark brown and deposited a black precipitate. We therefore carried out a comparison of the relative activities of the Karstedt catalyst and **11** over two successive runs (Figure 6).

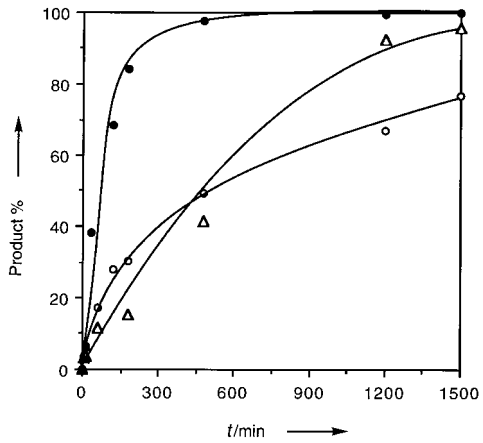

Figure 4. Activities of catalysts **2** (△), **5**(●), and **6**(○) in the hydrosilylation of triethylvinylsilane by triethylsilane at 30 °C with 6×10^{-6} mol of Pt catalyst.

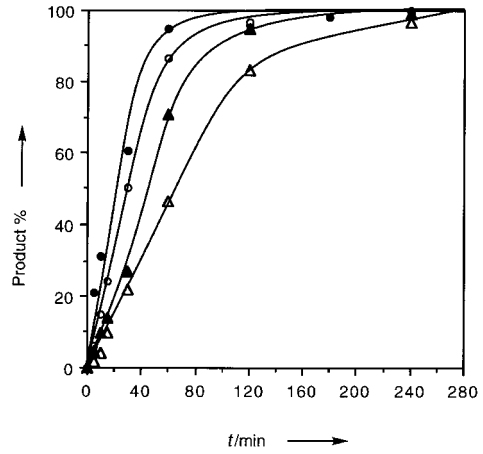

Figure 5. Activities of catalysts **7** (▲), **8** (△), **10** (○) and **11** (●) in the hydrosilylation of triethylvinylsilane by triethylsilane at 30 °C with 6×10^{-6} mol of Pt catalyst.

Table 3. Reactivities of the triolefinic complexes as catalysts in the hydrosilylation of trimethylvinylsilane by triethylsilane with 6×10^{-6} mol of platinum catalyst; $t_{1/2}$ is the time taken for 50% reaction.

Complex	Ligand	$t_{1/2}$ [min]
11	Methylnaphthoquinone (MeNQ)	22
10	Dichloronaphthoquinone (DCNQ)	30
7	Naphthoquinone (NQ)	45
8	TND	60
5	TETCE	60
6	Tetracyanoethylene (TCNE)	480
2	Fumaronitrile (FN)	585
1	Karstedt catalyst	65

After the initial typical run described above, further quantities (1000 equiv) of each of the substrates were added to the catalyst solutions. It is seen that within experimental error both catalysts were slightly less active on the second run but **11** remained approximately four times more active in terms of initial rates. This procedure was then repeated by addition of further aliquots of substrates to both catalyst systems. It was found that under these conditions the Karstedt system became inactive after approximately 2900 turnovers, whereas **11** finally produced about 4200 equivalents of

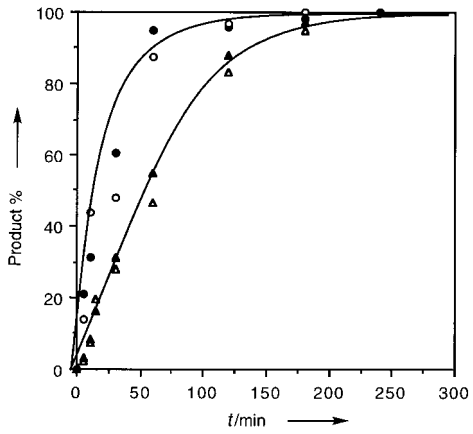

Figure 6. Activities of the first and second runs of the Karstedt catalyst (▲,△) and **11** (○,●) in the hydrosilylation of triethylvinylsilane by triethylsilane at 30 °C with 6×10^{-6} mol of Pt catalyst.

product. However over several runs the decrease in activity of **11** was gradually accompanied by a darkening of the solution with the formation of a black precipitate. We reasoned that the degradation of **11** may be occurring as a result of the loss of the stabilising MeNQ ligand and therefore studied the effect of the presence of excess MeNQ on the catalytic behaviour of **11**. Following the procedure of using successive substrate additions described above, the initial rates observed using 50-fold excess of MeNQ per Pt catalyst **11** were around 800 – 1000 turnovers h^{-1}, which were a little lower than those using **11** alone. However this activity was maintained over a much longer period, thus enabling a total turnover of ca. 26000 equiv per platinum atom. Furthermore, the colour of the catalytic solutions remained a clear yellow throughout. Increasing the additional MeNQ to 100 equiv had no further effect. The Karstedt catalyst solution contains an excess of dvtms which may reduce its efficiency somewhat but will also no doubt serve to stabilise the catalyst. Whatever the overall effect of the presence of excess dvtms on the Karstedt system may be, the productivity of **11** in the presence of excess MeNQ is more than ten times that obtained using the Karstedt catalyst under these conditions.

Tests on the catalytic reaction with mercury, dibenzo[*a,e*]cyclooctatetraene (DBCOT) and molecular oxygen:

a) Effect of mercury: The inhibitory effect of mercury on a catalytic reaction has been proposed as a test for the heterogeneous nature of the catalyst.[12] Mercury supposedly quenches the catalytic reactivity by forming an amalgam with the small platinum particles. Inhibition by Hg has been observed in a photoinduced hydrosilylation reaction using $CpPtMe_3$ as catalyst,[13] whereas when a surface-immobilised, monomeric, coordinatively unsaturated platinum species was involved, no inhibitory effect was seen.[14]

We found that when **11** was used as catalyst both the rate and final yield were unchanged in the presence of mercury (see Figure 7, left) which would indicate that catalysis using **11** was homogeneous throughout.

The Karstedt catalyst, under the same conditions, responded differently. In the presence of Hg, the catalyst was very active for a short period but the solutions became progressively more sombre and catalysis suddenly stopped at less than 40 % silane conversion (Figure 7, right). The Karstedt catalytic action appeared to involve two phases: an initial, active, possibly homogeneous phase that then yielded a heterogeneous system whose activity was inhibited by Hg.

b) Effect of DBCOT: It has been proposed that a phenomenological distinction between homogeneous and heterogeneous Pt catalysts can be also made by studying the effects on the catalytic process of strongly coordinating polyolefins such as DBCOT.[15] Such chelating diolefins coordinate strongly to molecular platinum(0) species, rendering them inactive in hydrosilylation or hydrogenation, whereas heterogeneous systems should be largely unaffected by their presence. Indeed using the Karstedt catalyst little lowering in rate was observed for up to 5 equiv of DBCOT, the reaction going readily to completion (Figure 8, right), indicating that the Karstedt catalyst is largely heterogeneous in action.

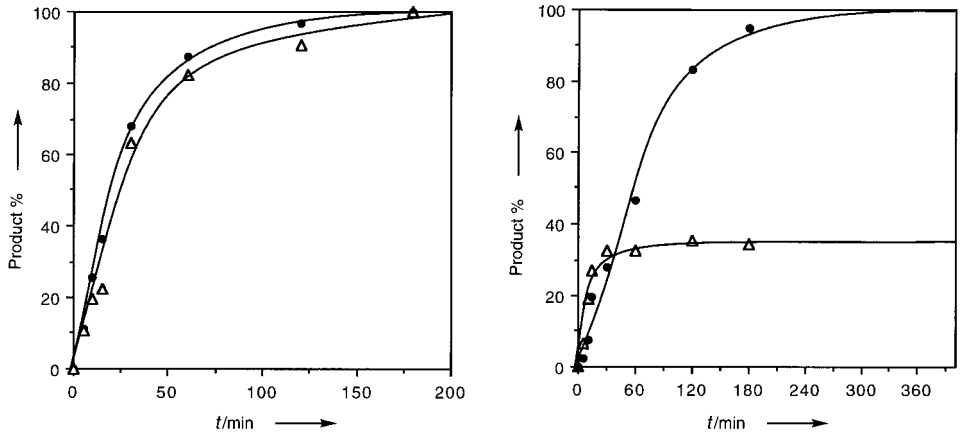

Figure 7. Effect of mercury on the Karstedt catalyst (right) and the catalyst **11** (left). Conditions: hydrosilylation of trimethylvinyl silane by triethylsilane: $T = 30$ °C; $[Si{-}H]_0 = 0.5$ mol L^{-1}; $[C{=}C]_0$: 0, 1.5 mol L^{-1} in hexane (20 mL); 6×10^{-6} mol Pt catalyst. With 0.1 mL Hg (△), without Hg (●).

However, the addition of DBCOT (1 equiv/Pt) to catalytic solutions of **11** (Figure 8, left) caused a decrease in the initial rate by ca. 30 % (cf. Figure 7) although the reaction still went to completion. However, in the presence of 5 equiv of DBCOT per equiv Pt, a further decrease in rate was observed and the catalytic reaction stopped at 60 % conversion.

c) Effect of molecular oxygen: It has long been known that molecular oxygen can have an important effect on hydrosilylation catalysis. It was observed that small quantities of oxygen induced high activity not only for Pt but also Rh

0947-6539/98/0410-2012 $ 17.50+.50/0 *Chem. Eur. J.* **1998**, *4*, No. 10

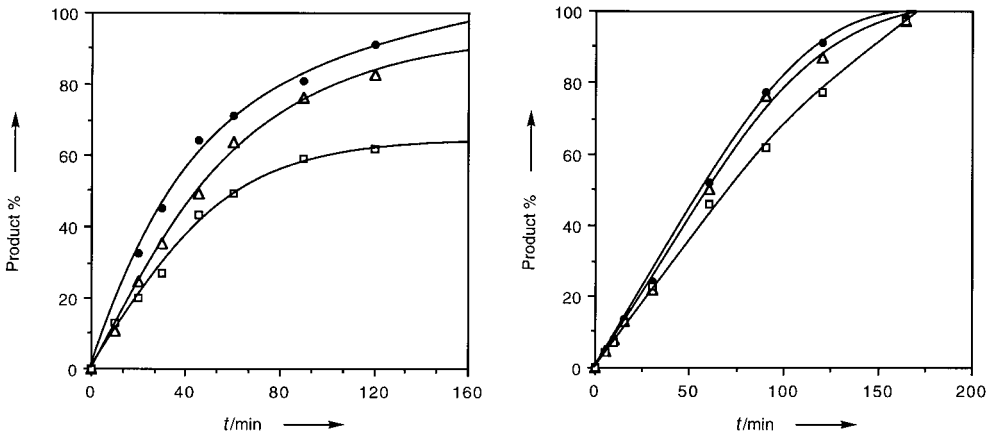

Figure 8. Effect of DBCOT on the Karstedt catalyst (right) and the catalyst **11** (left). Conditions: hydrosilylation of trimethylvinylsilane by triethylsilane: $T = 30\,^{\circ}C$; $[Si{-}H]_0 = 0,5\ mol\,L^{-1}$; $[C{=}C]_0$: 0, 15 mol L^{-1} in hexane (20 mL); 6×10^{-6} mol Pt catalyst; (●) 1 equiv DBCOT, (△) 2 equiv DBCOT, (□) 5 equiv DBCOT.

catalysts,[16] and Lewis[4] has suggested that O_2 is required both to generate and stabilise the active platinum colloids to prevent their further agglomeration into inactive species. In contrast, oxygen was found to inhibit a molecular hydrosilylation catalyst system dramatically.[14] In Figure 9 we compare the rates of hydrosilylation with **11** and with the Karstedt catalyst under three conditions, namely under argon, argon with ca. 1% O_2, and pure O_2 (1 atm).

Using **11** the presence of even a small quantity of O_2 significantly reduced the rate and under pure O_2 the reaction stopped at 40% completion. Little change occurred in the Karstedt system on addition of 1% O_2, but a significant lowering in rate was observed using large quantities of O_2. These observations differ somewhat from those previously reported, but since the conditions used also differ direct comparisons may not be valid.

Overall the evidence indicates that catalysed hydrosilylation using the molecular Pt^0 complex **11** is homogeneous in nature. There is certainly no evidence to the contrary. However the results concerning the Karstedt catalyst are less clear-cut and, in part, contradictory; it is possible that both heterogeneous and homogeneous processes are involved, as previously suggested by Lewis.[4]

Spectroscopic studies of the catalytic reaction: Colloidal particles of platinum absorb in the visible–ultraviolet in solution; Lewis has used this property to identify their presence and their size in the reaction solutions of the Karstedt catalyst.[4] We carried out a study at 40 °C using a hexane solution of $Me_3SiCH{=}CH_2$ (0.15 mol L^{-1}) and Et_3SiH (0.07 mol L^{-1}) to which a fixed quantity of catalyst was added with [cat]/[olefin] ≈ 1/1000. The reaction followed by UV/Vis spectroscopy and glc. With **11**, the reaction was complete (by glc) after 20 min and no appreciable absorption was detected at 500–600 nm. Interestingly, however, the MeNQ ligand absorptions in **11** at 380–400 nm were modified progressively with the appearance of an isosbestic point at 350 nm, indicating the formation of a new species in solution. We confirmed previous observations that on using the Karstedt solutions there was an increase of an intense absorption in the UV/Vis which increased with time (over 20 min), and analysis of the solutions at the end of the reaction by photon correlation spectroscopy (PCS) showed the presence of particles of mean diameter of ca. 400 ± 120 nm. However, when the catalytic reaction using **11** was carried out with lower [olefin]/[SiH] ratios (1 or less), a progressive darkening of the solution occurred and PCS studies at the end of the reaction showed in this case that particles (ca. 360 ± 100 nm) had been formed. It appears that using **11** the catalyst remains stable and homogeneous as long as there is sufficient stabilising ligand present to offset the detrimental effects of large silane concentrations.

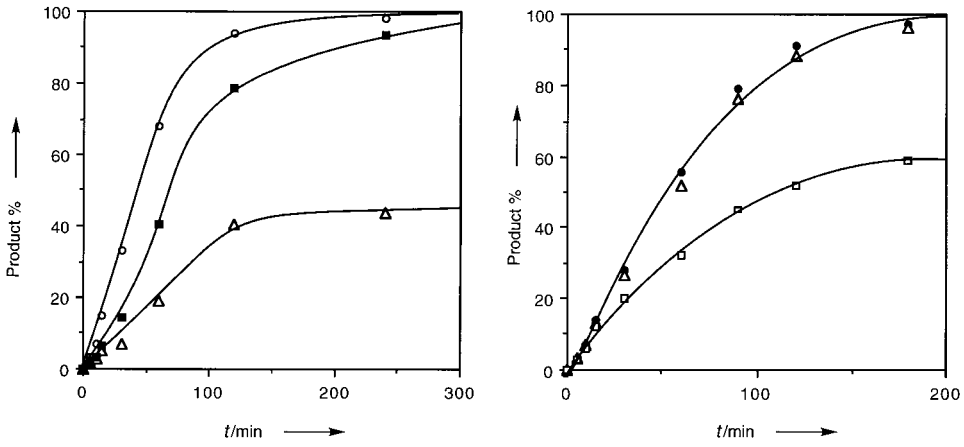

Figure 9. Oxygen effect on the Karstedt catalyst (right) and the catalyst **11** (left). Hydrosilylation of trimethylvinylsilane by triethylsilane: $T = 30\,^{\circ}C$; $[Si{-}H]_0 = 0,\ 5\ mol\,L^{-1}$; $[C{=}C]_0$: 0, 15 mol L^{-1} in hexane (20 mL); 6×10^{-6} mol of Pt catalyst. On right: (●) under Ar, (△) ca. 1% O_2 in Ar, (□) O_2 atm; on left: (○) under Ar, (■) ca. 1% O_2 in Ar, (△) O_2 atm.

NMR studies on the catalytic reaction: **^{195}Pt and ^{29}Si spectroscopies**: Pregosin[17] studied the hydrosilylation of [Pt(η^2-$PhCH{=}CH_2)_3$] by Ph_3SiH using ^{195}Pt and ^{29}Si NMR. The ^{195}Pt spectrum of [Pt(η^2-$PhCH{=}CH_2)_3$] exhibited two resonances at $\delta = -5904$ and $\delta = -5886$, corresponding to two isomeric forms which, on addition of excess Ph_3SiH, gave rise to further peaks at $\delta = -5010$ and $\delta = -5017$, each of which was coupled to one ^{29}Si nucleus. It was proposed that the complexes [Pt(η^2-$PhCH{=}CH_2$)(Ph_3Si)H]$_n$ or [Pt(η^2-$PhCH{=}CH_2$)(η^2-Ph_3Si-H)]$_n$ ($n = 1$

or 2) were formed in these reactions. In addition the complex [Pt(η^4-1,5-cyclooctadiene)$_2$] displays a ^{195}Pt resonance at $\delta = -4636$.[18]

We found that in CD_2Cl_2/CH_2Cl_2 at 203 °K **11** showed a sharp resonance in the ^{195}Pt{^{1}H} spectrum at $\delta = -4216$ ($\Delta\nu_{1/2} = 70$ Hz) as expected for a Pt^0 complex. In the ^{29}Si NMR of **11** in CD_2Cl_2 two ^{29}Si resonances of equal intensity were observed at $\delta = 3.22$ and 3.59, both coupled to a single ^{195}Pt with ^2J(Pt,Si) = 36 Hz. These observations are consistent with the solid-state structure being preserved for **11** in solution. No noticeable change occurred in the ^{195}Pt signal on the addition of small quantities of $Me_3SiCH{=}CH_2$ (10 equiv) but when a large excess (150 equiv) was added, a signal at $\delta = -4406$ appeared. Similarly, excess $PhCH{=}CH_2$ or $CH_2{=}CH{-}CH_2OAc$ caused peaks to grow in at $\delta = -4471$ and -4523, respectively. The ^{1}H-coupled ^{195}Pt spectrum of the styrene-rich solution exhibited a complex, apparent six-line structure (relative intensities ca. 1:2:3:3:2:1) with peak separations of ca. 40 Hz which clearly resulted from coupling of ^{195}Pt to several vinyl protons, but the lack of resolution did not allow the observation of any $^3J(Pt-CH_3)$ coupling. The corresponding ^{1}H spectrum showed several methyl resonances assignable to dvtms, including signals which coincided with uncomplexed dvtms. No evidence for displacement of the methylnaphthoquinone ligand was observed. Since the ^{195}Pt chemical shift was found to vary with the nature of the olefin substrate added, a minimum of one site on Pt^0 must be occupied by this olefin. Compound **A** (Scheme 2, with NQ as ligand drawn for simplicity) would appear to be a reasonable proposition for the species formed.

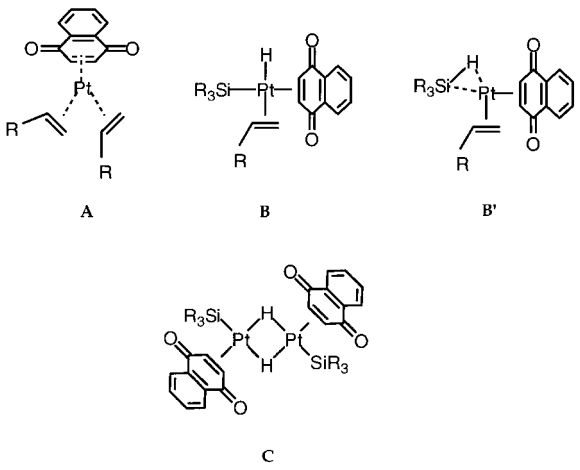

Scheme 2. Postulated intermediates in Pt^0-catalysed hydrosilylation with naphthoquinones as ligands.

When Et_3SiH (5 equiv) was added to the olefin-rich solutions (150 equiv olefin) of **11**, a low-intensity peak grew in at $\delta = -4233$, which was invariant in position with the olefin used and which only disappeared when all the silane was consumed. We tentatively propose this peak results from the formation of [Pt(η^2-MeNQ)(HSiEt$_3$)]$_n$ ($n = 1$ or 2, see **C**, Scheme 2), similar to the species originally proposed by Pregosin.

Temperature stability of the Pt catalysts: Under the standard conditions at 20 °C using **11** the catalytic reactions went smoothly to completion in ca. 24 h with an initial rate, $v_i \approx 10.8$ mmol L^{-1} h^{-1}. At 50 °C, v_i increased to 30.2 mmol L^{-1} h^{-1} but after 2 h the rate had greatly decreased with decomposition of the catalyst and only 68 % total conversion was finally obtained. At 73 °C, v_i was 48 mmol L^{-1} h^{-1} but very rapid decomposition immediately took place which led to a low overall conversion (18 %). Similar observations were made for the complexes **6** and **10**.

Synthesis and catalytic activity of [Pt(η^2-norbornene)$_2$(η^2-MeNQ)] (12): It may be asked at this stage whether the dvtms in the precursor complex **11** is retained as a ligand in the active form of the catalyst or is displaced from the metal before entry into the catalytic cycle. We therefore synthesised the analogous complex [Pt(η^2-nbe)$_2$(η^2-MeNQ)] (**12**, nbe = norbornene), and tested its catalytic activity. The yellow-ochre complex was prepared by the treatment of [Pt(η^2-nbe)$_3$] with MeNQ (Figure 10) and characterised by microanalysis and NMR spectra.

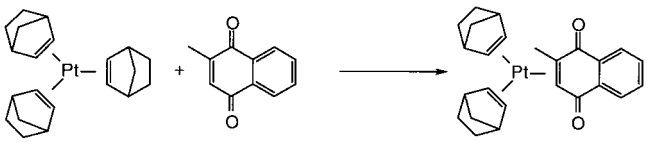

Figure 10. The synthesis of [Pt(η^2-norbornene)$_2$(η^2-(2-methylnaphthoquinone)].

The catalytic activities of **12, 11** and the Karstedt catalyst in the reaction of trimethylvinylsilane and heptamethyltrisiloxane are compared in Figure 11. At 50 % conversion the values

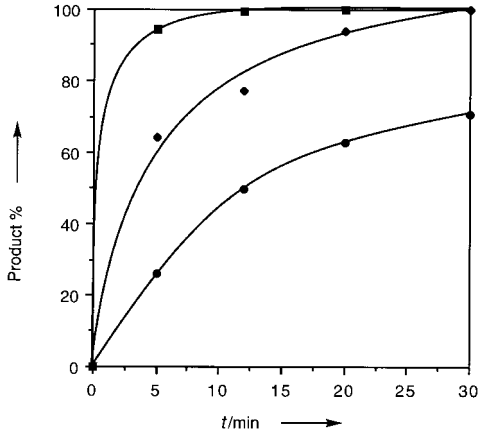

Figure 11. Hydrosilylation of trimethylvinylsilane by heptamethyltrisiloxane with the Karstedt catalyst (●), **11** (◆), and **12** (■); conditions as described in the Experimental Section.

of $t_{1/2}$ were ca. <1, 4 and 14 min, respectively, for the three catalysts; notably, the rate of reaction with **12** was considerably greater than that with **11**. The selectivity of silane addition was the same for both **12** and **11** (90 % α), slightly greater than that found for **1**.

0947-6539/98/0410-2014 $ 17.50+.50/0 *Chem. Eur. J.* **1998**, *4*, No. 10

The higher activity of **12** vis-à-vis **11** is probably a result of the greater lability of the norbornene ligand compared with dvtms which would generate the catalytically active species more readily under hydrosilylation conditions. Indeed we have found in a separate experiment that the norbornene ligands in **12** can be readily displaced by dvtms to form **11**. However, most of our studies used **11** rather than **12** because of the ease of its synthesis and high stability.

Discussion

In this paper we describe a family of Pt^0 catalysts, [Pt(η^2-olefin)$_2$(η^2-Ol_E)], where Ol_E is an electron-deficient olefin, which are efficient catalysts for the hydrosilylation of olefins. These compounds are readily synthesised and are easy-to-handle solids. Spectroscopic studies and an X-ray structural characterisation show that Ol_E is bound by a η^2-olefin interaction to Pt^0. The η^2-binding of the naphthoquinone Pt^0 complexes differs from the previously known quinone analogues where the η^4-coordination mode was observed. It was therefore expected that the analogous dihydronaphthoquinone compounds would also be stable; this was confirmed by their synthesis and use as catalysts.

The catalytic activities of this family of compounds, [Pt(η^2-Ol_E){(η^4-CH_2=CHSiMe_2)$_2$O}], varied greatly with the nature of Ol_E. Hence the fumaronitrile **2** and tetracyanoethylene **6** complexes were inefficient catalysts, being approximately ten times less active than the Karstedt catalyst itself under the same conditions, and thus can serve as inhibitors for the Karstedt system. However, surprisingly, all the naphthoquinone and dihydronaphthoquinone complexes, **7**–**11**, as well as the tetraester compound **5** were found to be more active than the Karstedt catalyst under the standard conditions used. The moderately π-acidic nature of the olefin function appears to induce stabilisation of the Pt species in the catalytic cycle without loss of catalytic activity. However, if this interaction becomes too strong, as in the complexes of the strongly π-acidic fumaronitrile or tetracyanoethylene ligands, the activity markedly diminishes. This is probably also the case for the dimethylfumarate and dimethylmaleate analogues which have been recently proposed as inhibitors for the Karstedt catalyst.[9] Although we find that complexes of moderately π-acidic olefins appear to provide the optimal catalyst systems there appears to be no simple quantitative correlation between the electron deficiency of the olefin and catalytic activity.

The effects of Hg, DBCOT and O_2 on the catalytic activity of **11** were consistent with homogeneous rather than heterogeneous behaviour. The corresponding tests on the Karstedt catalyst were somewhat more ambiguous, indicating the possible coexistence of both heterogeneous and homogeneous activity.

Although it is too early to propose a detailed mechanism for these catalysts, it is most reasonable to propose that the catalytic fragment [Pt (η^2-Ol_E)] remains throughout the catalytic cycle. ^{1}H and ^{195}Pt NMR studies on model reactions of the hydrosilylation process using **11** showed that the MeNQ remained coordinated to Pt whereas dvtms was readily displaced. Similarly we have found[19] that treatment of **11** with phosphine ligands causes the displacement of the dvtms ligand, MeNQ remaining bound. The dvtms ligands in the precursor catalysts **2**–**11** therefore serve as a convenient fashion to generate [Pt(η^2-Ol_E)] in solution. Addition of an excess of the Ol_E ligand can increases the stability and overall productivity of these catalysts with little sacrifice in rate.

The classical mechanism for hydrosilylation was proposed over thirty years ago,[20] and studies on the phosphine-modified catalysts[6] and NMR studies[18] have permitted this mechanism to be elaborated, in particular, by including dimeric intermediates. In Scheme 2 three possible intermediates of these catalysts are proposed based on our spectroscopic observations and by analogy with previous proposals. The Pt^0 complex [(η^2-NQ)Pt(η^2-RCH=CH_2)$_2$] (**A**) is formed by displacement of the labile dvtms ligands by the presence of excess olefin, RCH=CH_2, under catalytic conditions. The dissociation of one RCH=CH_2 ligand would give a 14e$^-$ Pt^0 species, which on reaction with the silane would yield either the oxidative addition product, **B**, or possibly **B′**, [(η^2-NQ)Pt(η^2-RCH=CH_2)(η^2-HSiR_3)], containing a σ-bonded silane ligand. Further loss of olefin from **B** (or **B′**) followed by dimerisation would lead to **C**. Preliminary kinetic data[19] indicate that both monomeric and dimeric species are probably involved in the catalytic cycle and **B** and/or **C** may then lead to products. Catalyst decomposition appears to result from the further reaction of **B** or **C** with excess silane. Since this would involve an oxidative process at Pt the greater stability of these complex catalysts (compared with the Karstedt system) may be the result of the enhanced electron-deficient character of the Pt centre resulting from the presence of the π-acidic olefin ligand.

In conclusion, although several compounds of this type were known prior to our work, their application as catalysts for hydrosilylation of olefins under mild thermal conditions had not been reported. In fact certain electron-deficient olefins had been used, paradoxically, as inhibitors for hydrosilylation catalysts. The Karstedt active species had also been generated photochemically from certain quinone complexes by photochemical labilisation of the quinone ligand. The search for appropriate ligands is an important aspect of molecular catalysis, but it is rather surprising to find an electron-deficient olefin as the ligand of choice. Given the existence of chiral naphthoquinones and the high activity of this family of molecular Pt catalysts under mild conditions, their application to enantioselective hydrosilylation can be envisaged. Further, as a source of relatively stable, unsaturated Pt^0 species these compounds may find use in synthesis and other catalytic reactions.

Experimental Section

General considerations: The preparation and handling of compounds were carried out under an argon atmosphere, using standard vacuum line and Schlenk techniques or a glovebox. All solvents were dried with the appropriate drying agents and distilled under a nitrogen atmosphere. Deuterated solvents were degassed by three freeze–pump–thaw cycles and dried over molecular sieves prior to use. NMR spectra were recorded on Bruker AM 300 (^{1}H, ^{31}P), and AM 400 (^{195}Pt, ^{29}Si) instruments.

Chemical shifts are reported in δ units (ppm) using the standard external references (TMS, H_3PO_4, Na_2PtCl_4). Infrared spectra were performed on a Perkin Elmer FTIR 1600 spectrometer. GC analyses of the products of the catalytic reactions were performed using a Hewlett – Packard series II 5890 gas chromatograph with a semicapillary column (HP-1, methylsilicon gum, 10 m × 0.53 mm × 2.65 mm). All GC-MS measurements were performed at the Mass Spectroscopy Service of the Chemistry Research Centre. Elemental analyses (C, H, O, Pt) were carried out at the Microanalytical Service of the Research Centre at Strasbourg or the CNRS Microanalytical Service at Vernaison (France). Photon correlation spectroscopic measurements were made with a Coulter N4 instrument. X-ray experimental data were collected on an Enraf – Nonius CAD 4F diffractometer using graphite-monochromated $Mo_{K\alpha}$ radiation ($\lambda = 0.71073$ Å) at 298 K.

Crystallographic data (excluding structure factors) for the structure reported in this paper have been deposited with the Cambridge Crystallographic Data Centre as supplementary publication no. CCDC-101813. Copies of the data can be obtained free of charge on application to CCDC, 12 Union Road, Cambridge CB2 1EZ, UK (Fax: (+ 44) 1223-336-033; e-mail: deposit@ccdc.cam.ac.uk).

Synthesis of the platinum complexes: The Karstedt catalyst was obtained by stirring a solution of $H_2PtCl_6 \cdot 6H_2O$ (500 mg, 1.22×10^{-3} mol) in H_2O (0.2 mL) at 50 °C with tetramethyldivinylsiloxane (5 g, 0.026 mol, 6.18 mL) for 4 h. After cooling to room temperature, the solution was neutralised by 500 mg of $NaHCO_3$ and filtered, yielding the so-called solution A. The platinum concentration in this solution was measured by atomic absorption. It was supposed that the platinum in such solutions was solely in the form of Karstedt catalyst and the quantities of Karstedt catalyst used in the syntheses of the compounds described below have been calculated on this basis.

[Pt(η^2-(NC)HC=CH(CN))\{(η^4-CH_2=CHSiMe$_2$)$_2$O\}] (**2**): Karstedt catalyst (500 mg, 5.26×10^{-4} mol) in solution A was stirred with fumaronitrile (82 mg, 1.05×10^{-3} mol) in toluene (10 mL). The colourless solution was heated at 60 °C for 5 min, and after cooling to ambient temperature, the solvent was removed in vacuo. The resulting white powder was washed with hexamethyldisiloxane (2 × 20 mL), then tetramethyldivinylsiloxane (2 × 4 mL). After decantation and filtration, the product was dried under vacuum. Yield: 180 mg (39 %). ^{1}H NMR (300 MHz, $CDCl_3$, 25 °C, TMS): $\delta = 3.5 - 5$ (m, 8 H, CH_2=CH and CH=CH), − 0.20, − 0.26(s, 3 H, $SiCH_3$), 0.42, 0.35 (s, 3 H, $SiCH_3$); IR (nujol): $\tilde{\nu}$ (cm^{-1}) = 2221 (CN), 1573, 1013 (CH_2=CH−Si), 1254, 833, 799 (Me_2Si−O); m.p. 130 °C (decomp).

[Pt(η^2-(EtOOC)CH=CH(COOEt))\{(η^4-CH_2=CHSiMe$_2$)$_2$O\}] (**3**): Diethylfumarate (158 mg, 9.20×10^{-4} mol) was added to the Karstedt catalyst (437 mg, 4.61×10^{-4} mol) in solution A. The solution was then warmed to 70 °C for 30 min. After cooling to − 78 °C, colourless crystals were collected, washed twice with cold pentane (5 mL) at − 78 °C and dried under vacuum. Yield: 134 mg (26 %); ^{1}H NMR (300 MHz, $CDCl_3$, 25 °C, TMS): $\delta = 3.5 - 4.1$ (m, 8 H, CH_2=CH), − 0.28 (s, 6 H, $SiCH_3$), 0.37 (s, 6 H, $SiCH_3$), 1.25 (t, 6 H, CH_3), 4.15 (q, 4 H, CH_2); IR (nujol): $\tilde{\nu}$ (cm^{-1}) = 1727 (C=O), 1259, 839, 794 (Me_2Si−O), 3040, 1000 (CH_2=CH−Si); m.p.: 127 °C (decomp); anal. calcd for C 34.71, H 5.46; found: C 35.20, H 5.60.

[Pt(η^2-(PhCO)CH=CH(COPh))\{η^4-(CH_2=CHSiMe$_2$)$_2$O\}] (**4**): Karstedt catalyst (215 mg, 2.3×10^{-4} mol) in solution A was concentrated under vacuum over 60 min in a Schlenk tube. *trans*-Dibenzoylethylene (108 mg, 4.5×10^{-4} mol) was added to the resultant oil. The mixture was then warmed to 75 °C for 15 min and, after cooling to − 78 °C, the resultant paste was washed with hexamethyldisiloxane (2 × 10 mL) and cold pentane (2 × 15 mL)(− 78 °C), yielding a white powder which was then dried under vacuum. Yield: 162 mg (57 %); ^{1}H NMR (300 MHz, $CDCl_3$, 25 °C, TMS): $\delta = 5.74$ (s, 2 H, ^2J(Pt,H): 60 Hz, CH=CH), 3.4 – 4.2 (m, 6 H, CH_2=CH), 0.28 (s, 3 H, $SiCH_3$), 0.23 (s, 3 H, $SiCH_3$), − 0.24 (s, 3 H, $SiCH_3$), − 0.62 (s, 3 H, $SiCH_3$), 7.5 and 8.2 (m, 10 H, Ar); IR (nujol) $\tilde{\nu}$ (cm^{-1}) = 1873 (CO), 1744 (CO), 1255, 836, 790 (Me_2Si−O), 3050, 1656, 1589, 1005 (CH_2=CH−Si); m.p.: 156 °C (decomp); anal. calcd for C 47.08, H 5.08; found: C 46.81, H 4.95.

[Pt\{η^2-(EtOOC)$_2$C=C(COOEt)$_2$\}\{(η^4-CH_2=CHSiMe$_2$)$_2$O\}] (**5**): The synthesis was carried out as for **4**. Yield: 102 mg (69 %); ^{1}H NMR (300 MHz, $CDCl_3$, 25 °C, TMS): $\delta = 3.7 - 5.2$ (m, 6 H, CH_2=CH), − 0.19 (s, 3 H, $SiCH_3$), 0.05 (s, 3 H, $SiCH_3$), 0.15 (s, 3 H, $SiCH_3$), 0.38 (s, 3 H, $SiCH_3$), 4.16 (q, 8 H, CH_2), 1.30 (t, 12 H, CH_3); IR (nujol): $\tilde{\nu}$ (cm^{-1}) = 1741 (CO), 1714 (CO), 1227, 837, 799 (Me_2Si−O), 1019 (CH_2=CH−Si); m.p.: 138 °C (decomp); anal. calcd for Pt 22.56; found: Pt 22.05.

[Pt\{η^2-(NC)$_2$C=C(CN)$_2$\}\{(η^4-CH_2=CHSiMe$_2$)$_2$O\}] (**6**): The synthesis was carried out as for **2**. The white solid obtained was dissolved in hexane, passed through a silica column and recovered as a white powder on removal of the hexane. Yield: 153 mg (51 %); ^{1}H NMR (300 MHz, $CDCl_3$, 25 °C, TMS): $\delta = -0.36$ (s, 3 H, $SiCH_3$), − 0.24 (s, 3 H, $SiCH_3$), 0.0 (s, 3 H, $SiCH_3$), 0.09 (s, 3 H, $SiCH_3$), 3.5 – 4.5 (m, 6 H, CH_2=CH); IR (nujol): $\tilde{\nu}$ (cm^{-1}) = 2234 (CN), 1573, 1028 (CH_2=CH−Si), 1261, 839, 799 (Me_2Si−O); ^{195}Pt\{^{1}H\} NMR (85 MHz, $CDCl_3$): $\delta = -3870$; anal. calcd for C 32.12, H 3.60; found: C 32.25, H 3.57.

[Pt(η^2-napthoquinone)\{(η^4-CH_2=CHSiMe$_2$)$_2$O\}] (**7**): Karstedt catalyst in solution A (437 mg, 4.61×10^{-4} mol) was concentrated under vacuum for 60 min in a Schlenk tube, and toluene (10 mL) was added to the resulting oil. Naphthoquinone (146 mg, 10^{-3} mol) was then added to the mixture and the green solution heated at 65 °C for 10 min. After cooling to room temperature, the mixture was stirred for 12 h. The solvent was removed under vacuum and the resultant powder was washed with tetramethyldivinylsiloxane (1 × 2 mL) and hexamethyldisiloxane (2 × 10 mL). The pale green solid was dried under vacuum. Yield: 230 mg (47 %); ^{1}H NMR (300 MHz, $CDCl_3$, 25 °C, TMS): $\delta = 4.95$ (s, 2 H, ^2J(Pt,H): 52 Hz), 3.3 – 4.2 (m, 6 H, CH_2=CH), − 0.92 (s, 6 H, $SiCH_3$), 0.15 (s, 6 H, $SiCH_3$), 7.9 and 7.5 (m, 4 H, Ar); ^{13}C NMR (200 MHz, C_6D_6): $\delta = -3.15$, 0.88 ((CH_3)$_2$Si), 60.1 (*C*H=CH−CO), 74.3 (*C*HSi), 76 (*C*H_2CHSi), 126, 132.9 (*C*H arom), 133.7 (C quinone), 186.53 (*C*O); IR (nujol) $\tilde{\nu}$ (cm^{-1}) = 1873 (CO) 1744 (CO), 1656, 1589 (CH_2=CH−Si) 1255, 836, 790 (Me_2Si−O); m.p.: 138 °C (decomp); anal. calcd for C 40.06, H 4.48; found: C 40.10, H 4.57.

[Pt(η^2-TND)\{(η^4-CH_2=CHSiMe$_2$)$_2$O\}] (**8**): (TND: 1,2,3,4-tetramethyl-4*a*,8*a*-dihydro-*endo*-1,4-methylmethanonaphthalene-5,8-dione: $C_{16}H_{19}O_2$) Karstedt catalyst in solution A (420 mg, 4.5×10^{-4} mol) was concentrated under vacuum for 60 min to obtain an oil. TND (225 mg, 9.1×10^{-4} mole) was then added and the solution heated at 70 °C for 30 min. After cooling to ambient temperature the resultant solid was washed twice with hexamethyldisiloxane (2 × 5 mL) and pentane (2 × 20 mL), then dried under vacuum, yielding a white powder. Yield: 345 mg (60 %); ^{1}H NMR (300 MHz, $CDCl_3$, 25 °C, TMS): $\delta = 3.5 - 4.0$ (m, 6 H, CH_2=CH), − 0.35 (s, 6 H, $SiCH_3$), 0.35 (s, 6 H, $SiCH_3$), 4.15 (s, 2 H, ^2J(Pt,H): 56 Hz, CH=CH), 2.09 (s, 2 H, 2 CH), 1.54 (s, 6 H, CH_3), 1.32 (s, 6 H, CH_3), 0.5 (d, 2 H, CH_2); IR (nujol) $\tilde{\nu}$ (cm^{-1}) = 1672 (CO), 1258, 839, 794 (Me_2Si−O), 1654, 1007 (CH_2=CH−Si); m.p.: 152 °C (decomp); anal. calcd for C 45.98, H 6.17; found: C 46.41, H 5.64.

[Pt(η^2-BAD)\{(η^4-CH_2=CHSiMe$_2$)$_2$O\}] (**9**): (BAD: 9,10-dihydro-9,10-*ortho*-benzenoanthracene-1,4-dione) The synthesis was carried out as for **8** but with a longer heating period (60 min at 70 °C) to obtain a white powder. Yield: 420 mg (68 %); ^{1}H NMR (300 MHz, $CDCl_3$, 25 °C, TMS): $\delta = 3.2 - 4.2$ (m, 8 H, CH_2=CH), − 0.38 (s, 6 H, $SiCH_3$), 0.35 (s, 6 H, $SiCH_3$), 7.1 and 7.4 (m, 8 H, Ar), 5 (s, 2 H, ^2J(Pt,H): 56 Hz, CH=CH), 2.45 (s, 2 H, 2 CH); IR (nujol): $\tilde{\nu}$ (cm^{-1}) = 1652 (CO), 1260, 835, 797 (Me_2Si−O); m.p.: 202 °C (decomp).

[Pt(η^2-2,3-dichloronaphthoquinone)\{(η^4-CH_2=CHSiMe$_2$)$_2$O\}] (**10**): The synthesis was carried out as for **8** to obtain a pale yellow powder. Yield: 381 mg (70 %); ^{1}H NMR (300 MHz, $CDCl_3$, 25 °C, TMS): $\delta = 3.6 - 4.2$ (m, 6 H, CH_2=CH), − 0.58 (s, 6 H, $SiCH_3$), 0.28 (s, 6 H, $SiCH_3$), 7.52 and 8.52 (m, 4 H, Ar); ^{13}C NMR (200 MHz, C_6D_6): $\delta = -2.75$ and 0.84 ((CH_3)$_2$Si), 85 (Cl*C*=*C*Cl), 82 (*C*H ligand), 133, 127 (*C*H arom), 206.9 (CO quinone); ^{195}Pt\{^{1}H\} NMR (85 MHz, $CDCl_3$): $\delta = -3100$; IR (nujol): $\tilde{\nu}$ (cm^{-1}) = 1677 (CO), 1591 (CH_2=CH−Si), 1259, 845, 800 (Me_2Si−O); m.p.: 152 °C (decomp); anal. calcd for C 35.53, H 3.64; found: C 36.18, H 3.65.

[Pt(η^2-methylnaphthoquinone)\{(η^4-CH_2=CHSiMe$_2$)$_2$O\}] (**11**): The synthesis was carried out as for **8** but with a shorter heating period (15 min at 70 °C) to obtain a pale yellow powder. Yield: 220 mg (78 %).Crystals suitable for X-ray analysis were obtained by recrystallisation from hexane. ^{1}H NMR (300 MHz, $CDCl_3$, 25 °C, TMS): $\delta = 5.04$ (s, 1 H, ^2J(Pt,H): 48 Hz, CH=C), 2.0 (s, 3 H, ^3J(Pt,H): 30 Hz, CH_3), 3.3 – 4.2 (m, 6 H, CH_2=CH), 0.27 (s, 6 H, $SiCH_3$), − 0.77, − 0.88 (s, 3 H, $SiCH_3$), 7.9 (td, 2 H, Ar), 7.5 (dd, 2 H, Ar); ^{13}C NMR (200 MHz, C_6D_6): $\delta = 132.8$, 132.3, 126.2, 125.6 (*C* arom), 185.4 (*C*O), 18.2 (*C*H_3 quinone), 0.92 – 3.12 (*C*H_3–Si), 66 (*C*=C), 74, 76 (CH_2 siloxane), 96 (CH siloxane); ^{195}Pt\{^{1}H\} NMR: (85 MHz, $CDCl_3$): $\delta = -4226$; IR (nujol): $\tilde{\nu}$ (cm^{-1}): 1655 (CO), 1594 (CH_2=CH−Si), 836, 791

0947-6539/98/0410-2016 $ 17.50+.50/0 *Chem. Eur. J.* **1998**, *4*, No. 10

(Me_2Si–O), 720 (C arom); m.p.: 144 °C (decomp); anal. calcd for C 41.95, H 4.76, Pt 33.83; found: C 41.81, H 4.77, Pt 33.70.

[Pt(η^2-norbornene)$_2$(η^2-methylnaphthoquinone)] (**12**): [Pt(norbornene)$_3$] (200 mg, 4.2×10^{-5} mol) and methylnaphthoquinone (72 mg, 4.2×10^{-5} mol) were stirred in toluene (20 mL) under an inert atmosphere and heated at 40 °C for 3 h. The solvent was then removed under vacuum and the resultant yellow-brown powder washed with pentane (2×10 mL) and dried under vacuum. Yield: 65 %; ^{1}H NMR (300 MHz, $CDCl_3$, 25 °C, TMS): $\delta = 3.6$ (s, 4H, CH=CH, ^2J(Pt,H): 66 Hz), 2.9 (s, 4H, CH), 1.7 (dd, 8H, CH_2), 1.2 (dd, 4H, CH_2), 7.9 (td, 2H, CH), 7.5 (dd, 2H, CH), 4.57 (s, 1H, CH=C (naphthoquinone) ^2J(Pt,H): 50 Hz) 1.87 (s, 3H, CH_3 (naphthoquinone) ^3J(Pt,H): 34 Hz); anal. calcd for C 54.05, H 5.08; found: C 54.22, H 5.17.

Catalytic studies: Hydrosilylation reactions were carried out in Schlenk tubes equipped with septum caps under an argon atmosphere at 30 °C. In a typical experiment, the platinum catalyst (6×10^{-6} mol) was transferred to a Schlenk tube and degassed hexane (30 mL) was added under argon. The solution was stirred for 5 min and the olefin (6×10^{-3} mol) and silane (3×10^{-3} mol) were then injected in quick succession from syringes through the septum. Samples were taken by syringe periodically for GC analysis. Based on one set of measurements the data were reproducible to ca. ± 5 %.

Mercury inhibition studies: Two solutions containing 6×10^{-3} mol of trimethylvinylsilane, 6×10^{-6} mol of catalyst and 30 mL of distilled *n*-hexane were degassed and then stirred for 60 min, one solution with 1.4 g of filtered Hg and the other without Hg. Et_3SiH (3×10^{-3} mol) was then added to both solutions and the hydrosilylation process was monitored by GC analysis.

DBCOT inhibition studies: Three degassed solutions containing 6×10^{-3} mol of trimethylvinylsilane, 6×10^{-6} mol of catalyst and 30 mL of distilled *n*-hexane were prepared and 1, 2 and 5 equiv of DBCOT per platinum atom, respectively, were added to these solutions. After 60 min, Et_3SiH (3×10^{-3} mol) was added. The hydrosilylation process was then monitored by GC analysis.

Oxygen effects: Three degassed solutions containing 6×10^{-3} mol of trimethylvinylsilane, 6×10^{-6} mol of catalyst and 30 mL of distilled *n*-hexane were prepared. The catalyst (6×10^{-6} mol) was then added to the solutions under argon. The first Schlenk tube was left under argon. In the second tube, a small amount of pure oxygen (ca.2 mL) was injected. The third tube was filled entirely with oxygen. The hydrosilylation processes were then monitored by GC analysis.

Acknowledgments: The authors thank Rhône Poulenc Silicones for generously supporting this work and for a gift of the Karstedt catalyst, and Dr Gerard Mignani for animated discussions.

Received: December 11, 1997 [F923]

[1] B. Marciniec, *Comprehensive Handbook on Hydrosilylation*, Pergamon Press, **1992**.

[2] a) J. L. Speier, J. A. Webster, G. H. Barnes, *J. Am. Chem. Soc.* **1957**, *79*, 974–979; b) J. L. Speier, *Adv. Organomet. Chem*. **1979**, 407–447.

[3] B. D. Karstedt (General Electric Co.) USP 226 928, **1972** [*Chem. Abstr.* **1974**, *80*, 16134j].

[4] a) L. N. Lewis, N. Lewis, *J. Am. Chem. Soc.* **1986**, *108*, 7228–7231; b) L. N. Lewis, EP 89105577.4, **1989**; c) L. N. Lewis, *J. Am. Chem. Soc.* **1990**, *112,* 5998–6004; d) L. N. Lewis, R. J. Uriarte, N. Lewis, *J. Catal*. **1991**, *127*, 67–74; e) L. Lewis, K. G. Sy, G. L. Bryant, P. E. Donahue, *Organometallics* **1991**, *10*, 3750–3759; f) L. N. Lewis, R. J. Uriarte, N. Lewis, *J. Mol. Catal*. **1991**, *66*, 105–113; g) L. N. Lewis, *Chem. Rev.* **1993**, *93*, 2693–2730.

[5] a) N. J. W. Warhurst, *Ph.D thesis*, University of Sussex, **1990**; b) P. B. Hitchcock, M. F. Lappert, N. J. W. Warhurst, *Angew. Chem*. **1991**, *91*, 439–441; *Angew. Chem. Int. Ed. Engl*. **1991**, *30*, 438–440.

[6] M. Auburn, M. Ciriano, M. Green, J. A. K. Howard, M. Murray, N. J. Pugh, J. L. Spencer, F. G. A. Stone, P. Woodward, *J. Chem. Soc. Dalton Trans.* **1980**, 659.

[7] G. Bennett-Stackhouse, L. L. Wright, *Inorg. Chim. Acta* **1988**, *150*, 5–8.

[8] M. J. Chetcuti, J. A. K. Howard, M. Pfeffer, J. L Spencer, F. G. A. Stone, *J. Chem. Soc. Dalton Trans.* **1981**, 276–283.

[9] L. N. Lewis, J. Stein, R. E. Colborn, Y. Gao, J. Dung, *J. Organomet. Chem*. **1996**, *521*, 221–227.

[10] M. F. Lappert, F. P. A. Scott, *J. Organomet. Chem.* **1995**, *492*, C11–C13.

[11] Crystallographic data for **11** are given in Table 1. Diffraction data was collected at room temperature on a Nonius CAD 4-F diffractometer with graphite-monochromated $Mo_{K\alpha}$ radiation. Cell constants and orientation matrix for data collection were obtained from a least-squares refinement using the setting angles of 25 carefully centred reflections. Collection was achieved using $\omega/2\theta$ scans to a maximum θ value of 26°. 9738 reflections were collected. Lorentz, polarisation and absorption corrections were applied to the data (absorption corrections from the ψ scans of 4 reflections). The structure was solved by the Patterson method. All non-hydrogen atoms were located by the heavy atom method, and were refined anisotropically. Hydrogen atoms, with the exception of the water protons, were introduced as fixed contributors with C–H = 0.95 Å, B(H) = 1.3 Beqv(C). The final cycle of full-matrix least-squares refinement was based on 4223 observed reflections ($I > 3\sigma(I)$) and converged with unweighted and weighted agreement factors of $R(F) = 0.033$ and $R(F)_w = 0.041$, respectively. All computations used OpenMolen on a DEC Alpha computer. [C. K. Fair in *MolEN, An Interactive Intelligent System for Crystal Structure Analysis*, Enraf–Nonius, Delft (the Netherlands), **1990**.] Crystal parameters, data collection details and results of the refinements are summarised in Table 2.

[12] G. M. Whitesides, M. Hackett, R. Brainard, J.-P. P. Lavalleye, A. F. Sowinski, A. N. Izumi, S. S. Moore, D. W. Brown, E. M. Staudt, *Organometallics* **1985**, *4*, 1819–1830.

[13] L. D. Boardman, *Organometallics* **1992**, *11*, 4194–4201.

[14] R. S. Paonessa, A. L. Prigano, W. C. Trogler, *Organometallics* **1985**, *4*, 647–657; A. L. Prigano, W. C. Trogler, *J. Am. Chem. Soc.* **1987**, *109*, 3586–3595.

[15] D. R. Anton, R. H. Crabtree, *Organometallics* **1983**, *2*, 855–859.

[16] F. De Charentenay, J. A. Osborn, G. Wilkinson, *J. Chem. Soc. A* **1968**, 787.

[17] A. Albinati, W. R. Caseri, P. S. Pregosin, *Organometallics* **1987**, *6*, 788–793; W. R. Caseri, P. S. Pregosin, *Organometallics* **1988**, *7*, 1373–1380.

[18] For a general survey see: P. S. Pregosin, *Coord. Chem. Rev.* **1982**, *44*, 247.

[19] P. Steffanut, J. A. Osborn, unpublished results.

[20] A. J. Chalk, J. F. Harrod, *J. Am. Chem. Soc*. **1965**, *87*, 16.

  0947-6539/98/0410-2017 $ 17.50+.25/0

flavylium ions upon a pH jump from 1.0 to 4.2 can be schematically represented as in Figure 11. In the case of 4′-hydroxyflavylium, $\mathbf{C_c}$ converts very slowly to $\mathbf{C_t}$, and thus **B**

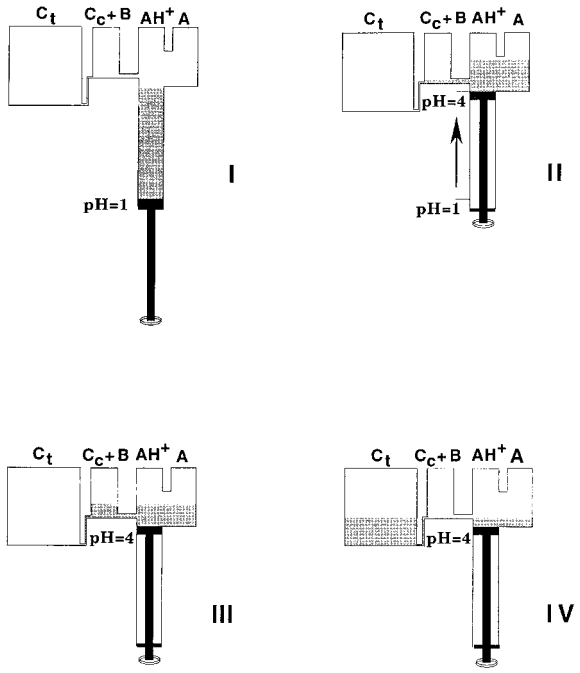

Figure 11. Hydraulic analogy for a pH jump from pH = 1.0 to pH = 4.0: I. The system is equilibrated at pH = 1.0. II. The system has been taken to pH = 4.0. The pH jump has an effect comparable to raising the piston; the figure represents the situation immediately after the proton transfer. III. When the *cis*→*trans* isomerization is very slow it is possible to obtain an intermediate (pseudo-equilibrium) state involving the species $\mathbf{A}H^+$, **A**, **B** and $\mathbf{C_c}$. IV. Thermodynamic equilibrium at pH 4.0.

and $\mathbf{C_c}$ accumulate; for 4′,7-dihydroxyflavylium and 7-hydroxyflavylium, however, $\mathbf{C_c}$ converts very rapidly to $\mathbf{C_t}$ so that $\mathbf{C_c}$ and **B** disappear as soon as they are formed.

The hydraulic analogy can also be used to illustrate the photochemical behavior of these compounds, light playing the role of a pump. The scheme shown in Figure 12 refers to 4′-hydroxyflavylium.

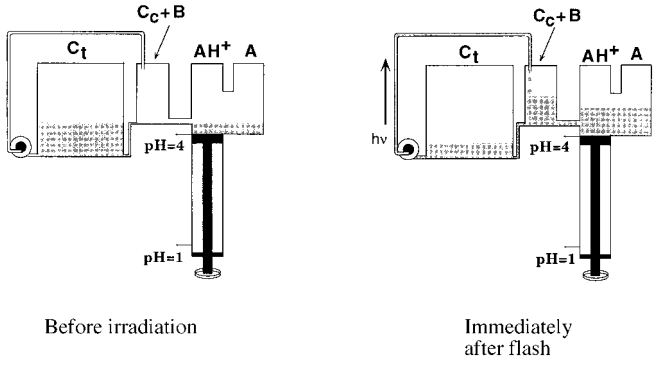

Figure 12. Hydraulic analogy for the photochemical reaction of $\mathbf{C_t}$. Light behaves like a pump that increases (in a transient mode as represented or in steady state) the quantity of liquid in the reservoir $\mathbf{C_c}$.

In a previous paper we showed that the 4′-methoxyflavylium ion can undergo a *write-lock-read-unlock-erase* photochromic cycle useful for information processing.[10] The different values of the rate constants, particularly in the case of the *cis*→*trans* thermal isomerization reaction, preclude this possibility for the 7-hydroxyflavylium and 4′,7-dihydroxyflavylium ions. In the language of photochromism, one can say that the information (color change) *written* by light excitation on the 7-hydroxyflavylium and 4′,7-dihydroxyflavylium derivatives *erases* spontaneously on a short time scale (seconds).

It can also be noted that, because of the competition between the pH-dependent rate of the reaction leading from the colorless $\mathbf{C_c}$ to the colored species $\mathbf{A}H^+$ and **A** and the pH-independent *cis*→*trans* back-isomerization, the amount of colored species formed upon light excitation depends on the pH of the solution. In other words, the pH of the solution plays the role of a tap for the color intensity generated by light excitation. This also means that this system can be viewed as a light-switchable pH indicator. In the case of 4′,7-dihydroxyflavylium the tap–color effect is larger than for 7-hydroxyflavylium.

Acknowledgments: This work was supported in Portugal by the Centro de Quimica Fina e Biotecnologia, Programa Plurianual, and in Italy by MURST and the University of Bologna (Funds for Selected Research Topics).

Received: February 4, 1998 [F984]

[1] R. Brouillard in *The Flavonoids, Advances in Research* (Ed.: J. B. Harborne), Chapman and Hall, London, **1988**.
[2] R. Brouillard in *Anthocyanins as Food Colors* (Ed.: P. Markakis), Academic Press, New York, **1982**, Chapter 1.
[3] R. Brouillard, J. E. Dubois, *J. Am. Chem. Soc.* **1977**, *99*, 1359.
[4] R. Brouillard, B. Delaporte, *J. Am. Chem. Soc.* **1977**, *99*, 8461.
[5] R. A. McClelland, S. Gedge, *J. Am. Chem. Soc.* **1980**, *102*, 5338.
[6] R. A. McClelland, G. H. McGall, *J. Org. Chem.* **1982**, *47*, 3730.
[7] P. Figueiredo, J. C. Lima, H. Santos, M. C. Wigand, R. Brouillard, A. L. Maçanita, F. Pina, *J. Am. Chem. Soc.* **1994,** *116*, 1249.
[8] a) F. Pina, L. Benedito, M. J. Melo, A. J. Parola, M. A. Bernardo, *J. Chem. Soc. Faraday Trans.* **1996**, *92*, 1693; b) R. Matsushima, M. Suzuki, *Bull. Chem. Soc. Jpn.* **1992**, *65*, 39; c) R. Matsushima, H. Mizuno, H. Itoh, *J. Photochem. Photobiol. A* **1995**, *89*, 251; d) R. Matsushima, H. Mizuno, A. Kajiura, *Bull. Chem. Soc. Jpn.* **1994**, *67*, 1762.
[9] a) M. Maestri, R. Ballardini, F. Pina, M. J. Melo, *J. Chem. Educ.* **1997**, *74*, 1314; b) F. Pina, M. J. Melo, R. Ballardini, L. Flamigni, M. Maestri, *New. J. Chem.* **1997**, *21*, 969; c) W. von Sperling, F. C. Werner, H. Kuhn, *Ber. Bunsenges. Phys. Chem.* **1966**, *70*, 530.
[10] F. Pina, M. J. Melo, M. Maestri, R. Ballardini, V. Balzani, *J. Am. Chem. Soc.* **1997**, *119*, 5556.
[11] F. Pina, A. Roque, M. J. Melo, M. Maestri, L. Belladelli, V. Balzani, *Chem. Eur. J.* **1998**, *4*, 1184.
[12] C. Michaelis, R. Wizinger, *Helv. Chim. Acta* **1951**, *34*, 1761.
[13] Universal buffer Theorell–Stenhagen, used in low concentration (0.05 M).
[14] P. K. Glasoe, F. A. Long, *J. Chem. Phys.* **1960**, *64*, 188.
[15] C. G. Hatchard, C. A. Parker, *Proc. R. Soc. London Ser. A* **1956**, *235*, 518.
[16] F. Pina, M. J. Melo, I. Abreu, J. C. Lima, H. Santos, R. Ballardini, M. Maestri, *New J. Chem.*, in press.
[17] *Photochromism—Molecules and Systems* (Eds.: H. Dürr, H. Bouas-Laurent), Elsevier, Amsterdam, **1990**.

  0947-6539/98/0410-2007 $ 17.50+.25/0